Title

Spatial integration during active tactile sensation drives orientation perception

Journal

Neuron, 109(10)

ISSN

0896-6273

Authors

Brown, Jennifer
Oldenburg, Ian Antón
Telian, Gregory I
et al.

Publication Date

2021-05-01

DOI

10.1016/j.neuron.2021.03.020

Peer reviewed

HHS Public Access

Author manuscript

Neuron. Author manuscript; available in PMC 2022 May 19.

Published in final edited form as:

Neuron. 2021 May 19; 109(10): 1707–1720.e7. doi:10.1016/j.neuron.2021.03.020.

Spatial integration during active tactile sensation drives orientation perception

Jennifer Brown[1,*], **Ian Antón Oldenburg**[1,*], **Gregory I. Telian**[2], **Sandon Griffin**[1], **Mieke Voges**[1], **Vedant Jain**[1], **Hillel Adesnik**[1,2,3]

[1]Department of Molecular and Cell Biology, University of California, Berkeley

[2]The Helen Wills Neuroscience Institute

[3]Lead contact

Summary

Active haptic sensation is critical for object identification, but its neural circuit basis is poorly understood. We combined optogenetics, two-photon imaging, and high-speed behavioral tracking in mice solving a whisker-based object orientation discrimination task. We found that orientation discrimination required animals to summate input from multiple whiskers specifically along the whisker arc. Animals discriminated the orientation of the stimulus *per se*, as their performance was invariant to the location of the presented stimulus. Populations of barrel cortex neurons summated across whiskers to encode each orientation. Finally, acute optogenetic inactivation of the barrel cortex and cell-type specific optogenetic suppression of layer 4 excitatory neurons degraded performance, implying that infragranular layers alone are not sufficient to solve the task. These data suggest that spatial summation over an active haptic array generates representations of an object's orientations, which may facilitate the encoding of complex three-dimensional objects during active exploration.

eTOC Blurb

hadesnik@berkeley.edu .

*Equal contributing authors

Author contributions

J.B. and H.A. conceived the study. J.B. conducted all the behavioral experiments. J.B. and I.A.O. conducted the imaging experiments. G.I.T. provided software for whisker tracking. S.G., V.J., and M.V. assisted in behavioral training and experiments. V.J. built the whisker contact detector. H.A., J.B., and I.A.O. wrote the paper.

Inclusion and Diversity

We worked to ensure sex balance in the selection of non-human subjects. One or more of the authors of this paper self-identifies as an underrepresented ethnic minority in science. One or more of the authors of this paper self-identifies as a member of the LGBTQ+ community. One or more of the authors of this paper self-identifies as living with a disability. One or more of the authors of this paper received support from a program designed to increase minority representation in science. While citing references scientifically relevant for this work, we also actively worked to promote gender balance in our reference list.

Declaration of interests

The authors declare no competing interests.

The integration of tactile input across active sensors is critical for perception. Brown, Oldenburg et al. show that mice summate tactile input from multiple whiskers in an arc to discriminate the orientation of an object. Correspondingly, populations of neurons in the barrel cortex integrate multi-whisker input to encode the orientation of objects and their activity is critical for task performance.

Introduction

To judge the shape, size and location of objects, cortical circuits must integrate information arriving from different parts of the sensor array, whether this be from different parts of the retina, the body surface, or the cochlea. Many animals, including humans, move their sensors to optimize information gathering, a process termed ‘active sensation’(Gibson, 1962). Humans use active sensation to investigate and manipulate objects by executing various stereotyped hand motions(Lederman and Klatzky, 1987). Tactile input from adjacent fingers conveys multi-dimensional information about the orientation and structural relationship of the object’s surfaces to give rise to a coherent object percept. In the primate somatosensory cortex, individual neurons can encode the orientation and curvature of a stimulus(Hsiao et al., 2002, DiCarlo and Johnson, 2000). Sensing the shape of an object, however, depends on dynamic integration of tactile input (i.e., skin indentation) with proprioceptive information about hand and joint position(Hsiao, 2008). How cortical circuits extract shape information during active sensation is poorly understood.

The rodent vibrissal system is a powerful model for active sensation and tactile perception, and the mouse offers the genetic tools that make dissecting the cellular and circuit basis of tactile perception possible(Petersen, 2019). Rodents sweep their whiskers across objects to localize and identify them(Ahissar and Knutsen, 2008, Diamond et al., 2008, Brecht et al., 1997). Judging object location and shape uses sensory circuits to integrate ex-afferent signals due to whisker contact and re-afferent signals due to self-generated whisker motion, conceptually analogous to proprioceptive input from the hand(Kleinfeld and Deschênes, 2011). Subsets of neurons in the barrel cortex integrate these two afferent streams to accurately localize stimuli in a head-centered coordinate frame(Diamond et al., 2008, Curtis and Kleinfeld, 2009). Rodents can readily identify and discriminate objects with their whiskers purely based on shape(Brecht et al., 1997, Anjum et al., 2006, Polley et al., 2005, Kim et al., 2020), and barrel cortex neurons are sensitive to the location(O’Connor et al., 2010, Sofroniew et al., 2015, Curtis and Kleinfeld, 2009), texture(Arabzadeh et al., 2003, Isett et al., 2018, Chen et al., 2013), shape(Anjum et al., 2006), deflection angle of individual whiskers(Kim et al., 2020, Bruno et al., 2003, Andermann and Moore, 2006, Lavzin et al., 2012, Simons, 1985, Kwon et al., 2018), and correlated motion of multiple whiskers across the whisker pad(Vilarchao et al., 2018, Jacob et al., 2008, Drew and Feldman, 2007). Discriminating some, but not all of these tactile features utilizes spatial summation over the whisker array (Pluta et al., 2017, Brumberg et al., 1996, Krupa et al., 2004, Kathleen Kelly et al., 1999). However, despite this work, the neural basis for orientation perception during active sensation, which may contribute to shape identification, is not understood.

To investigate the neural circuit basis of object orientation we developed an active whisker dependent orientation discrimination task for head-fixed mice, explored the behavioral and sensory basis of task performance, and measured neural activity in the barrel cortex as the mice solved the task. Object orientation discrimination required integration over vertically stacked whiskers, mice discriminated the object orientation *per se*, and calcium imaging revealed that neurons in the barrel cortex encoded all presented orientations of the stimulus, which required summation across whiskers. Inactivating the barrel cortex optogenetically, strongly impaired performance, and even much more selective optogenetic inactivation of layer 4 (L4) excitatory neurons reduced task performance. These data help define the circuits and computations that are required for the discrimination of object orientations during active sensation.

Results

Mice can use active touch to discriminate object orientations with high acuity

To probe the neural circuit basis of orientation perception, we developed a whisker dependent task that required mice to discriminate the orientation of tactile stimuli (Figure 1A,B). A stimulus bar was presented unilaterally to the mouse's right intact whisker field in one of eight possible orientations. Mice were trained to discriminate positive orientations (GO) and negative orientations (NOGO), licking for rewarded GO stimuli, but withholding licking to unrewarded NOGO stimuli (Figure 1C, S1). Mice routinely reached high levels of performance (d': 2.3±1.2 std, Figure 1E–H), performed high numbers of trials (301±89 std) and reached performance criterion (d'>1.5) after roughly one to two weeks of training (8.3±2.2 std days, Figure 1I). Mice readily discriminated orientations as small as 7° (Figure 1E–G), though further training may reveal even finer acuity. Even well-trained mice exhibited some licking for unrewarded NOGO trials. To test if this is an intrinsic perceptual bias towards such orientations or simply a bias towards licking, we trained a separate cohort of mice on the reverse orientation contingency. In these mice we also observed licking for NOGO orientations, strongly implying that the bias was a product of the operant training and not an asymmetry in perception (Figure S1F).

We developed a photo-interrupt touch detector to estimate the timing and the number of whisker contacts made with the stimulus bar before its decision (Figure 1C,D, S2). The mean latency from first touch to lick was around 400ms (full pad; 0.44±0.08s, 2 whiskers; 0.48±0.15s, std, Figure 1D, S2I). Mice made ~8 whisker contacts with the stimulus bar prior to licking (full pad; 8.5±1.4, 2 whiskers; 7.1±1.9, std, Figure S2J,K). We observed a tight coordination between whisking, running and licking behavior in trained mice during success trials: upon presentation of the stimulus all trained mice decelerated (most strongly to GO stimuli), adjusted their whisker set point caudally, and reduced their whisking amplitude in a stimulus dependent manner (Figure S3D,E). Naive mice showed modest, largely stimulus independent, changes in running and whisking, and no licking behavior (Figure S3B,C). These data indicate that multiple motor systems (running, whisking, and licking) were highly coordinated as a consequence of learning and successful performance in the task, implying a closed-loop process(Ahissar and Assa, 2016, Saig et al., 2012).

Orientation discrimination requires spatial summation across multiple whiskers

To probe how mice discriminate the orientation of the stimulus, we first confirmed the role of whiskers in task performance. Once mice had reached threshold and stable performance on the task, all whiskers were trimmed (~2mm length) preventing any contact with the stimulus bar. Trimming whiskers significantly reduced performance to chance levels (Figure 2B; $p<0.001$), confirming that mice solved the task through whisker touch and not through other sensory cues such as motor sounds.

We hypothesized that orientation perception may depend on integration over the whisker pad. Therefore, we asked whether contacts from multiple whiskers were required to solve the task. To address this directly, we measured performance as we acutely trimmed the whisker array to different combinations of whiskers (Figure 2A). We hypothesized that mice would require at least two whiskers, presumably in different rows (i.e., along an arc), to obtain relevant information on object orientation. Whiskers in different rows could discriminate positive from negative orientations by computing the relative horizontal position of object contact; in contrast, whiskers in the same row would only access the object at nearly the same elevation, and therefore have less information on object orientation.

Trimming the whiskers to a row of four or fewer significantly impaired task performance with discriminability dropping to chance levels (Figure 2C,E,F; $p <0.01$). In contrast, trimming to an arc of whiskers did not affect performance (Figure 2D–F; $p=0.74$). In fact, even just two whiskers in an arc was sufficient to perform the task (Figure 2D–F). Importantly, however, trimming to one whisker abolished performance (Figure 2D–F). These results demonstrate that mice solved the orientation discrimination task specifically by integrating multiple whiskers in an arc; contact information from a single whisker was insufficient. A similar study showed that mice with only one whisker can discriminate object orientation(Kim et al., 2020), perhaps by adopting alternative whisking strategies or by relying on the differing deflections of the remaining whisker. However, our data indicate that when trained with multiple whiskers in this task, the default strategy the mice use is to summate sensory information over at least two whiskers along an arc.

Mice can use the orientation of the stimulus *per se* to solve the task

Orientation perception should be invariant to the vantage point or absolute location of the object. Therefore, we next asked whether trained mice use the orientation of the stimulus bar *per se* to solve the task, rather than a more specific code that relies on contacting the stimulus bar with a specific set of whiskers in a specific location. Using high-speed whisker tracking data, we found that mice with intact whiskers contacted the stimulus bar primarily with their frontmost whisker arcs, and rarely made contact with the middle or back arcs prior to making their decision (Figure 3A). When these mice were acutely trimmed to a single middle arc of whiskers (Arc 2) they showed no significant drop in performance even though they had not been previously employing this arc to solve the task (Figure 3A). Thus, mice could immediately use these alternate whiskers to solve the task, indicating that they were employing a more general orientation-perception based strategy.

Next, we designed an experiment in a new group of mice that would not require whisker trimming. We hypothesized that if mice were using an orientation-based rather than a specific whisker/location-based strategy to solve the task, behavioral performance should be unaffected by acutely presenting the oriented stimulus bar in random horizontal locations within the whisking field. Thus, mice should discriminate the bar's orientation with different sets of whiskers on different trials. Therefore, we jittered the absolute horizontal location of the oriented bar, trial by trial, and monitored the effect on each mouse's performance. For these experiments, the stimulus bar was moved in from the side ('lateral presentation') rather than from the front to prevent the mice from solving the task while the stimulus bar was still moving towards its final position (Figure 3B). Although these mice were initially trained with the stimulus moving in from the front ('rostral presentation'), all mice quickly acclimatized to lateral presentation (1–3 days). Once they regained their original performance level, we began presenting the stimulus to one of three positions, each engaging different sets of whiskers. All three positions were randomly interleaved in the test session. Three out of five of the test mice maintained high levels of performance (d'>1.5) across all of the positions, strongly suggesting that these mice solved the task by sensing the stimulus orientation *per se* (Figure 3C,D). The other two mice showed a drop in performance only for the more distant position (pos2), which returned to baseline proficiency in 1–4 days. The transient drop in performance for these two mice might be due to the difficulty in acclimatizing to altered task conditions (multiple final locations of the stimulus), or to the need to re-learn new spatial rules for the two additional stimulus positions. The latter explanation would require them to solve the task by remembering three unique spatial coding rules, as opposed to a single orientation-based rule. These data show that mice can solve the task with multiple strategies, but that a majority of tested mice learn a more generalizable orientation-based rule.

To control for a strategy where mice adaptively adjust their whisking to different stimulus positions and thus are still able to solve the task with a spatial rule (in coordinates invariant to the whisking field), we tracked the motion of the whiskers with high-speed imaging. Whisker tracking showed that whisking properties were largely invariant across the different jitter positions (Figure 3E). Furthermore, high-speed video analysis showed that different whiskers primarily contacted the stimulus bar at each of the different jitter positions (Figure 3F). These results suggest that mice that showed no acute drop in performance when the stimulus bar was presented to different horizontal locations are using different sets of whiskers to determine the orientation of the stimulus bar and solve the task.

Barrel cortex neurons encode object orientation through spatial integration over the sensory array

Next, we sought to address the neural basis for object orientation discrimination. As we show that mice integrate over multiple whiskers to solve the task, we began by recording neural activity in the barrel cortex whose neurons integrate over the whisker array(Brumberg et al., 1996, Pluta et al., 2017, Krupa et al., 2004, Ramirez et al., 2014). We trained transgenic mice expressing GCaMP6s in excitatory neurons of the cortex on the task with a full whisker pad (camk2-tTa; tetO-GCaMP6s mice, Wekselblatt et al., 2016). Following training we imaged activity in the barrel cortex with volumetric calcium imaging, collecting

neural data from approximately 1,000 neurons per recording in 3 planes of ~800 × 800μm field of view (Figure S4A,B), encompassing several columns of the barrel cortex. We relied on 'Suite2P' for source extraction and neuropil subtraction (see Methods; Figure S4C–H, Pachitariu et al., 2016).

To explore the stimulus-evoked activity we analyzed calcium activity (both ΔF/F and deconvolved calcium (see Methods)) beginning at the estimated time of first whisker contact and extending to the end of the behavioral response window, 0.5 seconds prior to reward delivery (Figure 4A; see Methods and see Figure S5 where expanded and restricted time windows are considered). Across the imaged population of neurons, about 45% of identified neurons showed significant responses during presentation of the stimulus bar (see classification in Methods), and about one third showed significant tuning across the stimuli (Movie 1; Figure 4B–D). Importantly, we identified neurons in each mouse that responded best to each of the eight presented stimuli (Figure 4D, S6). This distribution of neuronal tuning across the discriminated orientations was robust as it was observable after cross-validation (Figure 4D, S7A) and visible across a wide range of analysis conditions (Figure S5A,B, S7B,C,D). We validated that the imaging resolution of our optical system was sufficient to resolve individual cells without cross-contamination (Figure S4C–J, and see Methods).

To quantify the selectivity of neural responses we computed a selectivity index (see Methods). Across all cells the selectivity index was much higher than shuffled controls or randomly generated data (Figure S7E; $p<1e-99$, rank sum test). Across the population of imaged neurons we observed a bias towards neurons encoding NOGO orientations, which may be due to earlier contact times with NOGO stimuli (Figure S2E,F,H), more contacts on NOGO trials (Figure S2G), different whisker kinematics following contact with the angled bar, other asymmetries in the stimulation or recording setup (Figure S3), or a physiological bias towards representing these orientations(Vilarchao et al., 2018). This overrepresentation was not dependent on task training since we also observed it in naive, untrained mice (Figure S5D). Despite this overrepresentation of cells selective for NOGO orientations, dimensionality reduction (see Methods) revealed that the population of imaged neurons smoothly represented and could discriminate all stimulus orientations (Figure 4E). In each recording, the population responses for each stimulus orientation diverged shortly after the estimated first whisker contact, indicating a high level of discriminability within the earliest touches (Figure S7F).

Although the barrel cortex exhibits topographic maps of whisker input(Woolsey and Van der Loos, 1970) and spatial input in the whisking field(Pluta et al., 2017), we did not observe any obvious organization of orientation selectivity, though we cannot rule out finer structure as further investigation is required. In all recorded mice, neurons with distinct tuning preferences appeared to be intermingled with each other (Figure 4F, S6), this observation was robust to the analysis window (Figure S5C).

We next asked how the animal's behavior and trial type modulated neural activity in the barrel cortex. While the stimulus bar's orientation was the strongest predictor of most neurons' responses in the task, trial type (GO vs NOGO), as well as motor decision (lick

vs no lick) also modulated the activity of many neurons, consistent with prior results(Yang et al., 2015) (Figure S8A). Furthermore, at their preferred stimulus orientation neuronal responses were slightly larger on trials where the animal responded correctly (Figure S8B; success trials: 0.28±0.004 vs failure trials 0.25±0.005 z-scored deconv. Ca^{2+} $p<10^{-34}$ rank sum test). However, this performance-based difference was much smaller than the difference between the presence and absence of a stimulus (Figure S8B). To compare the relative importance of different features of the task we employed a measure of absolute discriminability (see Methods). As this metric can be susceptible to low trial counts, we focused only on the middle four angles (±15°, ±7.5°) where there was a more even distribution of success and failure trials (mean: 11±2 failure trials, 23±2 success trials per condition, per mouse). We found cells that discriminated each tested features of the task (GO vs NOGO, lick vs no lick, success vs failure, or any orientation vs catch) at rates higher than in a shuffled control. However, cells were far more discriminative of the stimulus bar orientation (preferred orientation vs catch or vs least preferred) than any other comparison (Figure S8C,D, when computing scores that require a preferred orientation only cell's whose preferred orientation is one of the middle angles are included). This indicates that while the animal's behavior and task features modulate many neurons' responses, the stimulus orientation had the strongest influence on their physiological responses.

To determine if spatial summation(Simons, 1985, Kleinfeld and Delaney, 1996) across the whisker array was necessary for the orientation selectivity in the barrel cortex, in a subset of mice we acutely trimmed the mouse's whiskers from an arc of three to one whisker, a condition in which the mice fail to perform the task (see Figure 2). As a control, orientation tuned neurons were observed at similar rates and distributions in mice with three whiskers in an arc compared to mice with all whiskers intact (Figure 4G; S9; 37% tuned). However, when trimmed, we observed roughly half as many tuned cells, with some previously tuned cells becoming unresponsive (Figure 4G; top) and others losing their tuning (Figure 4G; below), leading to an increase in the proportion of responsive but untuned cells (Figure 4G; S9A–B; 20% remained tuned after trimming). Among the neurons that were both responsive in the three-whisker condition and after trimming, most tuned cells showed a decrease in orientation selectivity ($p < 1e\text{-}41$, rank sum test), whereas untuned cells remained untuned (Figure 4H; S9C; $p>0.32$, rank sum test). Further trimming to remove the last remaining whisker reduced task evoked activity to chance levels (Figure S9A,B). This implies that integrating across two or more whiskers is required for much of the object orientation coding in the barrel cortex in this task. This across-whisker summation might arise in the barrel cortex, or upstream, such as in the thalamus, where neurons show multi-whisker receptive fields(Timofeeva et al., 2004). Although barrel cortex neurons are well-known to encode angular deflections of single whiskers(Simons and Carvell, 1989, Bruno et al., 2003, Kim et al., 2020), here angular tuning alone appears insufficient for orientation coding and behavioral performance. Instead, these data imply that the mice used more global computations across the whisker array.

Orientation discrimination depends on neural activity in the barrel cortex

The data above show that mice learn to solve the orientation discrimination task by integrating touch information from multiple whiskers. Although neurons in the whisker

system as early as the trigeminal nucleus show sensitivity to multiple whiskers(Minnery and Simons, 2003), prior work(Brecht et al., 2003, Brumberg et al., 1996, Pluta et al., 2017) and our imaging data show that spatial integration is pronounced at the level of S1. Therefore, we tested whether neural activity in S1 would be required for task performance. Since studies have shown that the barrel cortex can be dispensable for tactile tasks(Hutson and Masterton, 1986, Hong et al., 2018), we inactivated S1 neural activity in several ways.

First, we suppressed excitatory neurons in the barrel cortex by virally expressing the potent inhibitory opsin eGtACR1 in emx1-Cre mice(Govorunova et al., 2015, Mardinly et al., 2018). An optic fiber coupled to a 470nm LED was positioned over S1 to illuminate all or nearly all of the barrel cortex. We randomly switched the LED on during one third of trials. To ensure silencing occurred before the first whisker contact, the LED was turned on one second before and remained on throughout the sampling and response window. Optogenetically suppressing excitatory neurons strongly reduced performance on the task (Figure 5A,E). Second, we photo-stimulated parvalbumin-positive (PV) GABAergic interneurons to silence nearly all barrel cortex activity by driving cortical inhibition(Sachidhanandam et al., 2013). This silencing likewise significantly reduced performance (Figure 5B,E). As a control, illumination in mice not expressing any opsin (WT) or targeted inactivation of the primary visual cortex (V1) had no impact on behavioral performance (Figure 5C–E). These results imply that barrel cortex activity is required for object orientation discrimination.

We observed that performance degradation was largely due to an increase in FA rates (Figure 5A,B). Perhaps because mice had a strong bias to lick across all stimuli from how they were trained (Figure S1), or because suppression of the barrel cortex directly induced licking. To address this issue, we first analyzed the impact of cortical suppression on catch trials, where the stimulus was not within reach of the whiskers. On these trials, barrel cortex suppression strongly increased the probability that mice would lick even though there was no contact between the whiskers and the stimulus bar (Figure 5A,B,F). Perhaps more importantly, the increase in the FA rate on catch trials predicted a corresponding increase in FAs for NOGO stimuli during optogenetic suppression but not in control mice (Figure 5A–D). This suggests that eliminating barrel cortex activity may have reduced the ability of mice not only to discriminate stimulus orientation but also to determine whether they were touching a stimulus at all. Next, we silenced the barrel cortex during inter-trial intervals (ITI) when there was no audible cue that a trial had been initiated (unlike catch trials when the stimulus did move but did not reach the whisking field). In contrast to catch trials, illumination of the barrel cortex during the ITI did not increase the probability of licking (Figure 5F). This shows that suppressing the barrel cortex did not directly induce the mice to lick in the absence of a contextual cues indicating the initiation of a trial. These data suggest that the GO/NOGO training paradigm we employed may have generated a strong bias to lick on trials when mice either could not discriminate stimulus orientation or could not determine whether a stimulus was present.

Although these results imply that barrel cortex activity is required for task performance, they provide no information on which sub-classes of cortical neurons might be important. Next, we specifically suppressed activity in a subset of layer 4 (L4) excitatory neurons with

the neuronal silencer eNpHR3.0 in scnn1a-Cre mice targeted to the barrel cortex (Figure 6A). Suppressing L4 excitatory neurons is a more subtle perturbation than cortex-wide inactivation; as we have previously shown, L4 suppression significantly degrades spatial representations in S1, but does not abolish sensory-evoked activity in any cortical layer(Pluta et al., 2015). We found that optogenetic suppression of a subset of L4 neurons significantly impaired performance, albeit more modestly than for total cortical inactivation (Figure 6A,C). In contrast, illumination of control mice not expressing any opsin had no effect on behavior (Figure 6B,C; WT). This demonstrates that L4 activity is required for normal behavioral performance, most likely either by driving sensory input to L2/3, or by sculpting activity in L5 through translaminar inhibition(Pluta et al., 2015). Together, these results imply that barrel cortex activity, *per se*, is necessary for object orientation discrimination.

Discussion

Using a tactile discrimination task we addressed how animals use active touch to discriminate object orientation. We propose that during natural object exploration, when many whiskers contact adjacent or overlapping surfaces, spatially distributed orientation-selective activity across many columns of the barrel cortex may give rise downstream to shape-specific neurons, akin to those found in the primate inferotemporal cortex(Perrett et al., 1982) that might be closely linked to object identification.

Since haptic perception in our task involves active whisker scanning, mice may have solved the discrimination task in a number of ways. Mice could use either ‘open loop’ or ‘closed-loop’(Ahissar and Assa, 2016, Saig et al., 2012) strategies to identify the object orientation. In an open-loop scheme, mice would not (or at least not need to) adaptively modify their whisking strategy to optimize orientation discrimination. One intuitive open-loop solution would be for neurons to compute the relative contact time with the oriented stimulus for each whisker. Contact time is known to be encoded both at peripheral levels(Jones et al., 2004, Leiser and Moxon, 2007) and in the cortex(Curtis and Kleinfeld, 2009, Waiblinger et al., 2015). Positive and negative lags of the relative contact time would thus indicate either positive or negative orientations, which in our paradigm indicate either GO or NOGO behavioral choices. Conversely, mice could adopt a ‘closed-loop’ strategy adapting their whisking kinematics across successive touches during a trial to optimize their stimulus orientation estimate(Saig et al., 2012, Ahissar and Assa, 2016). Whisker tracking revealed significant orientation-dependent changes in whisking kinematics including the whisker set point and amplitude following first contact with the stimulus. These changes were largely learned as they did not appear to the same magnitude or have the same orientation specificity in naive mice (Figure S2, S3).

Although it seems probable that different mice adopt different strategies, a significant fraction of mice seemed to perceive the orientation of the stimulus bar *per* se as acutely challenging them with the stimulus bar at different horizontal positions resulted in little to no drop in performance (Figure 3). Since mice could not perform the task with just one whisker, it also seems unlikely that mice simply computed the orientation of deflection of each whisker. Although with sufficient training they may adopt this strategy. Indeed, a recent study trained mice with one whisker to discriminate the angle of a stimulus bar and found

angular tuning maps in the barrel cortex(Kim et al., 2020). Thus, mice can determine the orientation of a contacted object with multiple strategies. Understanding the computations that mediate orientation discrimination should be a fruitful subject of additional work.

It is possible that some mice could have reduced the discrimination task to a detection task by adjusting their whisking strategy so that they only contact the stimulus bar for either the GO or NOGO stimuli. Our whisker and contact tracking do not support this scenario (Figure S2, S3). However, mice could adopt a whisking strategy where one whisker would only contact either GO or NOGO stimuli and only attend to whether this specific whisker made contact – reducing it to a touch-detection task. Since location coding is robustly encoded in the whisker system this is plausible(Knutsen et al., 2006, Knutsen et al., 2008, Ahissar and Knutsen, 2008). However, this seems to be unlikely since acutely trimming mice from a full whisker pad to an arc (trimming all but four whiskers) only slightly reduces performance (Figure 2) and jittering the azimuthal position of the stimulus did not reduce performance in most tested mice (Figure 3), which should have negated such a strategy. Therefore, the results more likely support the conclusion that the mice discriminate the different orientation *per se*, although a detection strategy cannot be ruled out.

Mice may discriminate the orientation of stimuli using the multipoint location of an object in space. Rodent whiskers move in a three-dimensional fashion that may facilitate precise location coding(Knutsen et al., 2008), and rodents can perform fine location discrimination with specific sets of whiskers(Knutsen et al., 2006). Different aspects of location representation are encoded in independent pathways(Knutsen and Ahissar, 2009) that likely converge in the barrel cortex, enabling barrel cortex neurons to faithfully encode this higher order feature. It is highly likely that the extraction of stimulus location must be essential to shape discrimination(Diamond et al., 2008). Our study supports the idea that the organization of whiskers involved in such extraction is critical, with an arc of whiskers carrying the richest information upon stimulus orientation or location when presented with a vertically orientated stimulus(Knutsen et al., 2006). If we had presented more horizontally oriented stimuli, contacts from different rows of whiskers might instead be most informative.

Importantly, with multiple approaches, we showed that normal activity in S1 is required for animals to discriminate object orientation in our task (Figure 5,6). S1 inactivation could impair performance because S1 activity encodes the surface orientation and passes this information downstream to generate the orientation-selective percept. Alternatively, S1 inactivation might simply disrupt activity in another region, such as the superior colliculus, that is more directly responsible for computing object orientation and passing this onto decision and motor execution circuits. Previously, focal inactivation or ablation of a specific sensory or motor area can lead to spontaneous recovery. This recovery could be explained by homeostatic rebalancing of activity in another brain region whose activity was disrupted by the lesion, or by the animals relearning the task with auxiliary circuits(Hong et al., 2018, Otchy et al., 2015). Although these are both difficult to rule out in our experiments, a more parsimonious explanation is that S1 activity and sensory computation in S1 *per se* are likely to be required, as S1 neurons encode the object orientations explicitly (Figure 4, S7). Finally, we found that degrading spatial representations in S1 via a much more subtle and partial L4-inactivation also impaired performance on the task (Figure 6), demonstrating that

normal L4 activity is required, or at least that activity in other layers is not sufficient. This lends additional support to the notion that S1 computation – putatively via L4 neurons - is necessary for object orientation discrimination.

Imaging S1 revealed that populations of neurons in S1 encoded all stimulus orientations in the task, and that much of this selective encoding depended on summation over multiple whiskers, as it largely disappeared in mice trimmed to a single whisker. We observed a large overrepresentation of neurons tuned to NOGO (−45°) orientations in expert (Figure 4; Figure S5) and naive (Figure S5) mice implying it was not a product of training but instead either related to kinematic differences in how the whiskers interact with the NOGO stimuli, or a biased representation of these stimuli in the cortex. During active whisking rodents palpate their whiskers against objects in a forward motion to induce whisker bending, vibrations and stick-slips(Isett et al., 2018, Hires et al., 2013, Arabzadeh et al., 2003, Jadhav et al., 2009). One explanation for the overrepresentation of NOGO stimuli could be that whiskers made a greater number of contacts and/or with higher force than with the GO (+45°) stimuli. To support this, we have shown that mice contact the −45° stimulus sooner than the other orientations resulting in a higher number of contacts during the initial decision period of the task. Furthermore, in a recent study, detailed kinematic analysis of whisker motion following contact with an oriented bar shows greatest vertical bending and displacement of the whisker following contact with more rostrally oriented bars compared to bars oriented more caudally(Kim et al., 2020). Interestingly, when we trimmed the whiskers down to a single C2 whisker, aligned with the fulcrum of the stimulus bar, we found a more even overrepresentation of −45° and 45° angles and an underrepresentation of intermediate angles. This is consistent with Kim *et al* in which detailed single whisker tracking showed that whisker contact with an +45° and −45° angled stimuli generates the greatest slide distances of the whisker compared to the intermediate angles, which may contribute towards such overrepresentations in S1(Kim et al., 2020).

Understanding how animals employ active sensorimotor strategies to optimize sensation and generate coherent percepts of the external world is critical for analyzing brain function and behavior. The head-fixed training paradigm we developed is simple but powerful – learning is quick and robust and can be probed by high-speed whisker tracking, and neural activity measurement and perturbation. Future experiments aimed at identifying the downstream circuits in the somatosensory system responsible for integrating multiple object orientations into a specific percept of a 3D object, will yield key insights into high level perceptual processes. Mice offer the most powerful genetic toolkit of any mammalian species, and like other rodents, presumably use high-resolution touch input to discriminate and identify small objects near their head. Therefore, mice trained on this and similar tactile tasks might yield fundamental insights into the neural mechanisms of higher order shape perception.

STAR Methods

RESOURCE AVAILABILITY

Lead contact: Further information and requests for resources should be directed to the Lead Contact, Hillel Adesnik (hadesnik@berkeley.edu).

Materials availability: All animal strains used in this study are available from Jackson Laboratories. All viral vectors are available from Addgene. All design files for custom fabricated parts are available upon request. No new strains or viral vectors were produced for this study.

Data and Code and Availability: All data and analysis software are available on request.

EXPERIMENTAL MODEL AND SUBJECT DETAILS

Animals—Mice used for experiments in this study were either wild type (WT (n=29 males); CD-1 (ICR) white strain, Charles River), PV-IRES-Cre (Jax stock# 008069) crossed with Rosa-LSL-ChR2 (n=9 males; PV-Cre⁖Ai32) (Jax stock# 012569), emx1-IRES-Cre (n=3 females, 3 males; JAX stock# 005628), scnn1a-tg3-Cre (n=8 females, 4 males; Jax stock# 009613), or tetO-GCaMP6s (Jax stock # 024742) crossed to Camk2a-tTA (n=4 females, 3 males; Jax stock# 003010). For Scnn1a-Cre;eNPHR3.0 (n=8 females, 4 males) and emx1-Cre;eGtACR1 (n=3 females, 4 males) there was no significant difference of the effect of light between males and females ($P>0.05$, t-test). Mice were housed in cohorts of five or fewer in a reverse light:dark cycle of 12:12 hours, with experiments occurring during the dark phase.

METHOD DETAILS

Headpost surgery—All experiments were performed in accordance with the guidelines and regulations of the Animal Care and Use Committee of the University of California, Berkeley. For head fixation during behavioral and physiological experiments, a small custom stainless-steel headplate was surgically implanted. Briefly, adult mice (P35-P50) were anesthetized with 2–3% isoflurane and mounted in a stereotaxic apparatus. Body temperature was monitored and maintained at 37°C. The scalp was removed, the fascia retracted, and the skull lightly scored with a drill bit. Vetbond was applied to the skull surface, and the headplate was fixed to the skull with dental cement (Metabond). A fine-point marker was used to note the approximate location of bregma and the left primary somatosensory barrel field (S1; 3.5mm lateral, 1.5mm posterior to bregma) and/or left primary visual cortex (V1; 2.7mm lateral, 0mm posterior to lambda), to guide the placement of optical fibers above the skull during optogenetic manipulations. Mice received buprenorphine and meloxicam for pain management and could recover for at least three days before being placed on water restriction.

Cranial window surgery—For imaging experiments, a second similar surgery was performed to implant a cranial window over S1. Briefly, mice were anesthetized as above, a 3–3.5mm region of skull located by stereotaxic coordinates (3.5mm lateral, 1.5mm posterior to bregma) was removed using a dental drill (Foredom) with a 0.24mm drill bit (George Tiemann & Co.) and/or a biopsy punch (Robbins Instruments). The window was replaced with three glass coverslips (two 3mm and one 5mm) and cemented into place with dental cement. Mice were given additional saline during surgery (0.3ml 0.9% NaCl). Mice were not water deprived at the time of surgery and were given several days to recover before water deprivation resumed. Mice received buprenorphine and meloxicam for pain management and dexamethasone to reduce brain swelling.

Viral infection—Neonatal emx1-IRES-Cre (P3–4) or scnn1a-tg3-Cre mice (P4–5) were injected intracranially with ~150–200nl of AAV9-CAG-DIO-nls-mRuby3-IRES-ST-eGtACR1 (eGtACR1) or AAV9-EFla-DIO-eNPHR3.0-EYFP (eNPHR3.0) respectively. With respect to the lamba suture coordinates were: 1.8–2mm anterior, 2.5–3mm lateral, 0.3mm ventral. Neonates were briefly cryo-anesthetized and placed in a head mold. Viruses were acquired from or custom produced at the University of Pennsylvania Vector Core.

Water restriction—Initial animal weight was recorded for 3 days before water restriction to establish baseline weight. Mice were then placed on controlled water and received 1.0ml/day of water. On training days, mice received most water during the task. Mice were weighed after training and given additional water if their weight dropped below 80% initial weight. Food was available *ad libitum*. The weight and health (quality of the fur and nails, gait, posture) of the mice were monitored daily.

Behavioral apparatus—The behavioral apparatus was controlled in real time by an Arduino Mega 2560 or Due, which interfaced with custom written software in Java. Mouse running velocity was measured via an incremental encoder (US Digital). Mouse licking was detected with a custom 2-transistor circuit between the 0.05-inch diameter steel tube lickport and a stainless steel headpost of the mouse(Slotnick, 2009). Whisker contacts were detected using a custom designed sensor attached to a 3D printed stimulus bar emitting an infrared (IR) beam that when broken by a whisker was recorded by the IR photodiode as a voltage deflection (see below). Water was delivered by gravity through a lickport under solenoid valve control (Neptube Research Inc.). A linear bar (25 × 3 × 1mm) was coupled to a stepper motor (NEMA 8; ‘stimulus motor’) via a custom cylindrical arm. The stimulus motor was mounted at 90° to a larger stepper motor (NEMA 17; ‘position motor’). The entire apparatus was mounted on an 8.0 × 8.0 × 0.5 inch (Thorlabs) anodized aluminum breadboard and enclosed in a light isolation box (80/20). Negative reinforcement was delivered via a single puff of compressed air, gated by a solenoid valve, to the contralateral eye from the whisker stimulus bar through a 0.05-inch-diameter steel tube positioned ~2mm from the eye. Air puff pressure was increased until it produced a blink response by the mouse. An optical fiber coupled to an LED (M470F3 or M617F2, Thorlabs) was placed on a separate manipulator above the mouse’s head and attached to a driver (LEDD1B, Thorlabs). On sessions with photo-stimulation, the fiber was positioned over the approximate locations of S1 or V1, as close to the thinned skull as possible. A masking LED light to minimize behavioral detection of the optogenetic light was also used on every trial during photo-stimulation sessions. The masking light was positioned directly in front of the mouse’s eyes and would turn on each trial for 1 second preceding and 1 second during the response window.

Behavioral task design—The orientation discrimination task followed the classical GO/NOGO paradigm (Figures 1 and S1). Head-fixed mice were trained to lick when they detected a GO stimulus and withhold licking when they detected a NOGO stimulus. Mice were presented with stimuli in one of eight possible orientations, defined by their angular position in the vertical plane. The eight stimulus orientations were ±45°, ±29°, ±15°, or ±7° from the dorsal-ventral axis. Except for the reversal contingency experiment (Figure S1), GO stimuli were oriented in the posterior direction and arbitrarily defined as positive

orientations. NOGO stimuli were oriented in the anterior direction and defined as negative orientations. On each trial, stimulus orientations were chosen at random subject to the constraint that all eight stimulus orientations be presented once in each block of eight trials, and not in a sequence of more than three GOs or three NOGOs in a row. On a subset of trials (10%), catch trials were randomly presented whereby the stimulus stopped just anterior to the mouse and outside of the whisker field.

The sequence for each trial was as follows (Figure S1). Each trial began with the stimulus in the home position for a 3–5 second waiting period. During this period, the stimulus motor rotated the stimulus bar to one of the possible pseudo-randomly selected orientations. After the waiting period, mice initiated the start of each trial by exceeding a ~50cm running requirement. This triggered the positioning motor to move the stimulus to the target position, within reach of the whiskers, except for catch trials whereby it was held just outside of the whisker field. The trajectory of the stimulus was aligned in roughly the same horizontal plane as the C row whiskers of the mouse's right whisker field, and centered around whisker C2. The distance between the stimulus and the whisker pad was 10.5 ± 0.3mm from follicle pad, n=10. For jitter experiments, the stimulus bar was attached to a linear stage and moved in laterally from the mouse whisker pad. The stimulus bar was jittered 20.6 ± 1.2° for first contact and 39.1 ± 0.9° at its final resting position relative to the mouse's whisker pad. Because the target position was in the approximate midpoint of the whisker field, mice typically made their first whisker contact with the stimulus before it reached the target position (Figure 1C,D, S2). Once stationary in the target position, mice were trained to either lick or withhold licking during a 1 second response window. The reinforcement schedule was as follows (Figure S1): correctly licking for a GO orientation (Hit) was rewarded with a drop of water (~5μl) 0.5 seconds after the response window ended. Incorrectly licking for a NOGO orientation during the response window (false alarm; FA) immediately triggered an air puff and a 5-second time-out period was added to the waiting period at the end of the trial. Correctly withholding licking to NOGO orientation (correct rejection; CR) were not rewarded and incorrectly not licking for GO responses (Miss) was not punished. All licks were recorded but licks outside of the response window had no consequences. At the end of the response window, the positioning motor moved the stimulus in reverse out of the whisker field and back to the home position. The exact location of the home position randomly jittered each trial by ±2cm radially so that the mouse could not predict catch trials based on the time in which the motor was moving. Once in the home position a random time-out period was given if the last trial was a false alarm.

Behavioral training—Training began after headplate application, recovery (~3days), and 5–10 days of water restriction. We did not find it necessary to handle the mice extensively before training or anesthetize them before head-fixation. Prior to training with the behavioral apparatus, mice were habituated to head-fixation on a free-spinning circular treadmill (diameter, 6 inches) for 4 daily sessions lasting ~60 minutes each (these run training days were not included when calculating number of sessions mice took to reach criterion (Figure 1I)). The training schedule was as follows (Figure S1): in the first stage of behavioral training ('$1Ori_{auto}$'), mice were classically conditioned to lick in response to the stimulus. The stimulus was only presented in the most extreme GO +45° orientation (or −45° on

the subset of experiments conducted with the reverse GO/NOGO contingency). On each trial, stimulus presentation was paired with a drop of water delivered 0.5 seconds into the response window. Once mice were reliably licking before the water was delivered (i.e. showing anticipatory licking on >70% of the trials), they were moved onto the operant conditioning phase of training.

In the second stage of training (‘1Ori’), mice were operantly conditioned to lick in response to the stimulus bar and withhold licking during the no stimulus, catch trials (10% of trials). The stimulus bar was only presented in the GO +45° (or −45° for reverse contingency experiments) orientation. A water reward was delivered only if mice licked during the response window to the GO stimulus. Once mice reliably licked upon detection of the stimulus and withheld licking to catch (>70% correct), they moved onto the simplest stage of the discrimination task (‘2Ori’). For both ‘1Ori $_{auto}$’ and ‘1Ori’ training mice could be moved onto the next stage of training within a training session if they performed above 70% correct for >100 trials to not over train the mice on this preparatory detection task.

During ‘2Ori’ discrimination training, mice were conditioned to lick only for GO trials (+45° or −45° for reverse contingency experiments) and withhold licking to NOGO (−45° or +45° for reverse contingency experiments) stimuli. GO and NOGO trials were randomly interleaved and catch trials were still presented on 10% of trials. A water reward was delivered on GO trials only if mice licked during the response window. In contrast, an air puff and time-out period were delivered if mice licked to the NOGO stimulus. When mice performed >70% for two consecutive days they were advanced to the final stage of the discrimination task (‘8Ori’). During ‘8Ori’, 4 GO and 4 NOGO stimuli were randomly presented to the mouse: ±45°, ±29°, ±15° and ±7°, and catch. Mice had to achieve >1.5 d’ (performance criterion) during ‘8Ori’ training to be used in subsequent experiments.

Mice were trained 5–7 days per week. All mice had a full pad of whiskers during training and for experiments unless otherwise stated. All sessions on ‘2Ori’ and ‘8Ori’ were preceded with ~10–20 trials on ‘1Ori$_{auto}$’ to ensure the lickport was positioned correctly and to prime mice for training.

Whisker tracking—A high-speed camera (Basler acA2000–340km) was placed below the running wheel; whiskers were imaged from below using a telecentric lens (Edmund Optics NT58–257) and a mirror oriented at approximately 45°. Some mice and experimental setups required slight adjustments to the mirror orientation to properly view the whiskers and object interaction. Whiskers were backlit from above using high-powered diffused infrared LEDs (CMVision-IR200). High-speed videos were acquired with a frame grabber (Silicon Software) at 500 frames per second with a 100μs exposure and were synchronized with behavioral data via external triggers. Whisker tracking was performed offline using Whisk (Janelia Research Campus, Howard Hughes Medical Institute), which returned whisker angles and positions for every frame. The whisker angle is in reference to the longitudinal axis of the mouse where 0° is fully retracted pointed towards the rear of the mouse, 90° is orthogonal to this axis, and 180° is fully protracted pointing directly forward. Typical whisker angles range from 70° at rest and 160° during a typical full protraction. Tracking data was further processed and analyzed using custom MATLAB scripts written to extract

set point and amplitude. Briefly, set point was calculated as the average of the upper and lower peak envelope of the orientation signal and amplitude was the difference between the upper and lower peak envelope. To define the sample analysis window for all except the Calcium imaging experiments (see later), we estimated first contact time as the period following a 2 standard deviation change in average baseline run velocity or set point (whichever occurred first) and estimated the end of the sample window as the start of average licking response (30% rise in lick rate from baseline). We then broke the trial into five 200ms analysis windows; baseline (#1: 500ms before first contact (#2)), the start (#2; corresponding to the estimated time of first contact), middle (#3; midpoint between first contact (#1) and first lick (#4)), end (#4; corresponding to the estimated time of first lick for expert mice, or the deviation in running velocity back to baseline for naive mice) and response time (#5; 500ms after first lick (#4)).

For jitter experiments, a subset of high-speed whisker tracking videos were manually annotated to identify which whiskers (front (arcs 4–6), middle (arcs 2–3) or back (arcs 1&G)) primarily contacted the stimulus bar. Each visually identified contact before the stimulus bar stopped moving into position (to estimate the 'decision period') was annotated. Only contacts where the mouse was actively whisking at the bar were included. Whiskers passively contacting the bar or being bent as the bar moved into position were not included in analysis. The most frequent (mode) whiskers making contact with the bar was calculated for each trial.

Whisk contact annotation validation—For manual whisker contact validation, two experimenters blind to experimental conditions annotated the same 10% of the data; if the interrater reliability (IRR) was less than 90%, experimenters discussed annotation approach and criteria. A new test data set was then selected, and the procedure repeated until >90% IRR was achieved. The remaining data was then annotated by either one or both experimenters.

Whisker contact detector—Whisker contacts were quantified in a subset of sessions using a custom designed sensor. The sensor was attached to a 3D printed stimulus bar emitting an infrared (IR) beam that when broken by a whisker or multiple whiskers was recorded by the IR photodiode as a voltage deflection (Figure S2). The raw voltage signal from the photodiode was baseline subtracted and smoothed. A contact was detected when a whisker or multiple whiskers occluded the sensor causing a voltage change in the photodiode that exceeded a given threshold. A threshold was calculated for each session as 3 standard deviations from the mean of the baseline period (−1 to −0.6 seconds before response period). Each contact in theory would generate two threshold crossings (one during protraction when the whisker or whiskers contact the stimulus bar and a second during retraction when the whisker or whiskers retract away from the stimulus bar), therefore putative contacts were calculated as the mid-point between sequential threshold crossings. For multi whisker data, whiskers frequently moved in synch and therefore would generate just one contact for multiple whiskers, therefore we used multi whisker data to describe multi whisker contacts, or 'whisks', as opposed to individual whisker contacts. To this end, threshold crossings spaced less than 20ms apart were averaged together to generate a single

contact. Trials that started below threshold or crossed threshold but did not return to baseline (largely caused by whiskers maintaining contact with the stimulus bar rather than actively pulsing at the bar) were excluded.

We validated the accuracy of the contact detector via two methods: piezo validation and high-speed video validation. For piezo validation, a single mouse whisker was plucked and tethered via glue onto a computer controlled piezo bender (Noliac Systems, NDR6110–100). Whisker deflections were controlled by custom written scripts in MATLAB that varied the frequency of deflections, and the whisker was positioned at different horizontal locations along the stimulus shaft to vary the distance of whisker deflection from the IR beam. The detected contacts were compared to the piezo output pulses. A true hit occurred when there was a contact detected within ±5ms from a piezo pulse. We found the detector was 100% accurate in detecting contacts for all the frequencies and positions tested. A second validation was conducted with an awake mouse performing the orientation discrimination task with two whiskers while simultaneously imaging the whiskers using high-speed video. *Post hoc* two human observers manually annotated a subset of trials and marked each frame whereby they observed a whisker or multiple whiskers contacting the stimulus bar. A threshold crossing within ±20ms of an annotated whisker contact was identified as a Hit. No threshold crossings within ±20ms of an annotated whisker contact was a Miss, while more than 1 threshold crossing within ±20ms of an annotated whiskers contact was identified as a False Alarm. Agreement between human observers was 98.3%. Hit rate comparing video annotations and contacts was 96%. We further annotated first contacts, defined by the first contact observed of a whisker or whiskers with the stimulus bar, and compared this with contacts identified with the sensor. The hit rate for first contacts was lower at 77%. We believe this higher error rate might arise from the difficulty in manually identifying first whisker contacts due to the reduced visibility as the stimulus bar moves into the whisker field, and the smaller degree of whisker bending we regularly see for first whisker contact. Therefore, we believe the higher error rate largely reflected observer error rather than error of the contact detector, and this was reflected in the larger rate of disagreement between human observers (80%).

Whisker trimming—A subset of mice had their whiskers ipsilateral to the stimulus either abruptly trimmed from full pad to no whiskers, or progressively trimmed from a full pad to four adjacent whiskers either in the same row (C1-C4) or arc (B2-D2), then to two adjacent whiskers either in the same row (C1-C2) or arc (B2-C2), then to one whisker (C2), and finally no whiskers. Once mice reached ‘8Ori’ criterion, mice were tested for two sessions prior to trimming to determine baseline performance. After each subsequent trimming procedure, mice were tested with the resulting configuration of whiskers over two sessions. For the progressive trimming group, mice were randomly assigned to the row or arc whisker conditions. When trimming from a full pad to four whiskers, mice were briefly anesthetized with 2–3% isoflurane after the second full pad session to eliminate any lingering impact of being under isoflurane. All other trimmings were done while mice were head-fixed and running on a treadmill.

Calcium imaging—Calcium imaging experiments were performed in mice expressing GCaMP6s in excitatory neurons via tetO-GCaMP6s × Camk2a-tTA or intracranial injection of AAV9 syn-GCaMP6s (titer 8e11 vg/mL) (Figures 4 and S4–9). After reaching training proficiency, mice were implanted with a cranial window on the side contralateral to stimulus presentation and following recovery they were returned to training for several days before being moved to an identical behavioral training apparatus connected to a two-photon microscope (Sutter MOM, Sutter inc.). Mice were given an additional 1–3 training days on the microscope rig to acclimate to the new environment. As two-photon microscopes provide many additional distractors to trained mice (e.g., temperature, sounds, environment) we reduced our d' criterion for inclusion to 1.0 (60% of recordings passed this threshold). Imaging fields of view were identified by manually deflecting whiskers and navigating towards areas with substantial, broad GCaMP fluorescence. Subsequent recording days were placed such that the same cells would not be recorded in separate days. All recordings were performed in L2/3 imaging three 800 × 800 μm planes, spaced 30–50μm apart, at 5.2–6.2Hz with ~100mW 920nm laser light (Coherent Chameleon) using a resonant galvo system. Images were acquired using ScanImage (Vidrio Inc.) with custom behavioral control software. Tiff files were motion corrected, cell masks were determined, and source fluorescence and OASIS(Friedrich et al., 2017) deconvolved signal data was extracted using Suite2p(Pachitariu et al., 2016). To confirm our imaging system has sufficient resolution to independently distinguish tuned neighbors, we measured the optical point spread function (PSF) of our imaging system and determined it to have a radial resolution of 0.49μm and axial resolution of 3.4 μm (Figure S4I) which is smaller than our pixel sampling, demonstrating that the optical resolution of our microscope is not a limiting factor, and supporting the notion that fluorescence from one cell is unlikely to contaminate any but the closest pixels due to the two photon excitation system itself. To quantify any cross-contamination between cells, we plotted the spatial distribution (i.e., distance to nearest neighbor) between tuned cells (Figure S4J; top) and all other cells (Figure S4J; bottom). We find that no cell pairs are closer than the optical performance of our microscope. Furthermore, we looked to see how many cells are unexpectedly close to each other, i.e., occurring closer together than a typical cell's width. We found that less than 0.25% of tuned pairs and 0.5% of any pairs of cells are closer together than the average width of a cell (determined to be 7μm radius in our data). This analysis implies that the vast majority of our cells should have little contamination from signals coming from the cell bodies of other cells.

As GCaMP6s has slow kinetics relative to the underlying changes in spike rate(T. W. Chen et al., 2013), we focused our analysis on a period after the animal's whiskers had made contact with the object but before the animal had made a behavioral response. For each recording, we identified the imaging frame in which the animal began slowing down, which was highly correlated with the first whisker touches (see Figure S2, S3). This frame, until the end of the 'response window' (i.e., when the stimulus leaves the whisker field), is called the standard window and was used for subsequent analysis (Figure S4).

We analyzed calcium responses both with ΔF/F and OASIS deconvolved Ca^{2+} activity; both methods gave qualitatively similar results (see Figure S4) and relied on Suite2p for data

extraction and calculation. For all methods, a weighted pixel mask for each cell was created based on the correlation of nearby pixels over time. Pixel masks were manually categorized as ‘cells’ or ‘not cells’ and only ‘cells’ were included for analysis. For ΔF/F calculation, each cell’s detected fluorescence was first neuropil subtracted. The average fluorescence of an anulus (not containing another cell) of up to 350 pixels was considered neuropil. A neuropil coefficient (c) was calculated for each cell as described in(Pachitariu et al., 2016) and the final fluorescence was calculated as

$$F = F_{cell} - c * F_{neuropil}$$

F_0, the ‘baseline’ fluorescence, was calculated with a moving average of the 10^{th} percentile of a 1000 frame window (approx. 3 minute); this moving average corrected for very slow drift in imaging conditions. ΔF/F is

$$(F - F_0)/F_0$$

Finally, as the absolute value of ΔF/F spans a wide range (likely due to differences in F_0), for display purposes each cell’s activity was scaled via z-scoring across the time series and pre-stimulus activity was subtracted. Each cell was processed independent of all other cells; thus, this operation could not affect calculated tuning preference or statistical significance. To demonstrate how this source extraction code operates on imaging data, we take two contrasting FOVs from the same recording as examples: one FOV where we have high signal from one cell adjacent to a few lower signal cells (Figure S4C–E), and a second where we have low mean signal from many cells within close proximity of one another (Figure S4F–H). In both cases we see that the ROI masks are not contaminated by neighboring cells and allow the extraction of clear, isolated responses from each of the cells. Deconvolved calcium activity was calculated using the OASIS algorithm(Friedrich et al., 2017), implemented in Suite2p(Pachitariu et al., 2016). This estimated the time and number of spikes that led to the observed calcium fluorescence. As with ΔF/F the absolute magnitude of estimated spikes varied widely, as such each cell’s response was z-scored across time and baseline subtracted. Analysis was based on the mean Z-scored deconvolved calcium activity from the standard window unless otherwise noted.

A trial was excluded if its run speed before stimulus presentation deviated more than 2 S.D. from its mean run speed. Tuned cells were defined as cells whose evoked responses to each oriented stimulus passed an ANOVA $p<0.01$, and these cells were further divided by their peak response. If a cell responded more on the catch trials than to any stimulus it was categorized as a suppressed cell. Touch cells were defined as cells that were not tuned but passed an ANOVA $p<0.01$ to all orientations and the catch trial. In all Calcium Imaging based figures error bars denoted a 95% confidence interval. Cross-validated tuning curves were calculated from the mean deconvolved activity (unless otherwise noted) and scaled from 0 to 1. Alternating trials from each cell were assigned to a sort group or a display group and tuning curves were calculated from each group. The order of the cells was set by the tuning preference from the sort group while the tuning curve from the display group was presented. Cells were excluded from this plot if the correlation between their sort group

tuning and display group tuning was < 0.5 (of the main data set 2960/3416 87% tuned cells pass this threshold). Principal component analysis (PCA) was performed on the full unrolled deconvolved calcium activity traces of every cell per experiment and subsequent responses were averaged by stimulus condition. Maps of tuning preference were presented as the projection of all three imaging planes with the outline of each detected source color coded by preferred tuning or touch responsive category. Orientation selectivity was calculated as the Euclidean Norm of the mean response to each oriented stimulus. As it is difficult to be certain what 0 activity looked like in calcium data, this response vector (v) was normalized from minimum to maximum activity. A selectivity of 1 would denote a response to only one orientation, whereas a selectivity of 0 would denote the same response to all stimuli. Selectivity

$$\text{Selectivity} = 1 - \frac{\left|\sqrt{\sum v^2} - 1\right|}{\sqrt{N} - 1}$$

ROC analysis was performed as previously described (Stüttgen and Schwarz, 2008). Briefly: single trial calcium responses were separated into two groups, A and B. Thresholds spanning the entire range of values in either group were tested, and the rates at which either group was above a given threshold were plotted against each other. The area under this curve (AUC) represented the discriminability. In this analysis it was irrelevant if A was larger than B or vice versa as we reported the absolute discriminability or |AUC-0.5|. Here 0 represented identical distributions whereas the maximal value 0.5 indicated that A and B were non overlapping distributions. As this metric can be biased by low trial counts, if A or B had fewer than 10 observations then that score was excluded. The shuffle control in this section was created by randomly sampling A and B groups from all observed trials. To be even more conservative, the number of samples in A and B were matched to the fewest samples in any of the comparisons for that cell.

In trimming experiments, intrinsic imaging was first performed to identify which whisker was optimally located in the cranial window for imaging. Whiskers were then trimmed to a column of three whiskers and the experiment began as described above, including manually deflecting the remaining whiskers to find areas with large GCaMP responses. Roughly half-way through a typical recording session, the whiskers above and below the principle imaged whisker were trimmed to create the single whisker recording set. As mice were unable to perform the task with a single whisker, recordings were included only if the animal had a performance accuracy d' of 1.0 or higher on the three-whisker condition, but all trials (success and failures) were included in analyses.

Intrinsic imaging—Intrinsic optical imaging was performed through the cranial window to confirm that either the C1 and/or the C2 barrel was located within the window to guide trimming for calcium imaging experiments. Prior to intrinsic optical imaging, anesthesia was induced as described above and mice were administered 0.01mg/kg Xylazine. Anesthesia was maintained with 1% isoflurane during imaging. Images were acquired at 60Hz with a 12-bit 1M60 camera (DALSA DS-21-01M60) and microscope fitted with two 52mm camera lenses (Nikon 52) using custom-written MATLAB software. The brain was illuminated with

red (630nm) LEDs. The C2 and/or C1 whisker was threaded through a wire loop connected to a Noliac piezo bender (Noliac Systems, NDR6110-100) and deflected at 20Hz for 4 seconds for 15 trials with a 6 second inter-trial interval. Mice were given 24 hours to recover.

Optogenetic stimulation *in vivo*—For optogenetic experiments light was delivered via a 400μm diameter optical fiber resting on the thinned skull over S1 or V1. Either a 470nm LED (M470F3, Thorlabs) at 8–12mW (for eGtACR1 expressing or PV-Cre::Ai32 mice) or 617nm LED (M617F2, Thorlabs) at 15–18 mW (for eNpHR3.0 expressing mice) was used. Light intensity was controlled by analog outputs to the LED driver (LEDD1B, Thorlabs) and calibrated with a photodiode and power meter (PM160T, Thorlabs). For behavioral experiments, a square light pulse was applied for 2 second intervals. To ensure photoinhibition before the first whisker contact and throughout the response window, optogenetic stimulation started 1 second prior to the stimulus reaching the target position and was sustained until the end of the response window. Optogenetic stimulation trials were randomly chosen on 33% of all trials. A masking light (blue for eGtACR1 and PV-Cre::Ai32 experiments, red for eNpHR3.0 experiments) was used to control for LED stimulation on all trials and an eye patch was positioned over the right eye of the mouse to prevent any visual cue which may have been gained through the masking light.

Histology and image acquisition—Transgenic and virally injected mice were anesthetized with 5% isoflurane and ketamine and perfused transcardially with 4% paraformaldehyde (PFA). Their brains were removed, stored overnight in 4% PFA at 4°C, and then cryoprotected for at least 24 hours in 30% sucrose buffer solution at 4°C. A sliding microtome (American Optical Company) was used to take 40μm coronal sections of S1 and/or V1. Sections were mounted on glass microscope slides using Vectashield mounting medium with DAPI to non-selectively stain cells and protect tissue from photobleaching. Sections were imaged using a confocal microscope with both a 4X and 20X air objective.

Behavioral data analysis

$$\text{Percent correct} = 100 * \left(\frac{Hit}{Hit + Miss} + \frac{CR}{CR + FA} \right) / 2$$

was used during training to advance mice through each stage of training. Discriminability index (d') was used to more precisely evaluate the ability of the mice to discriminate between GO and NOGO stimulus orientations. In calculating d', Hit Rate and false alarm Rate,

$$\text{Hit Rate} = {Hit}/{Hit+Miss}$$

$$\text{FA Rate} = {FA}/{FA + CR}$$

are considered. More precisely, d' is a measure of the difference between the z-transforms of Hit rate and FA Rate:

$$d' = z(Hit\ Rate) - z(FA\ Rate)$$

The effective limit of d' is 6.93, typical values are around 2.0, and we selected 1.5 as our performance criterion for reliable discrimination. Chance levels of discriminability corresponded to d'=0. We reported overall d' values for a complete session as well as d' for pairs of GO/NOGO stimuli whose orientations were equal and opposite. For the analysis of lick probability, we quantified the proportion of trials for each stimuli where mice made a GO response. The psychometric curve of lick probability was fit with a Wichmann and Hill psychometric fit.

If a mouse failed to make GO responses for 32 consecutive trials, we assumed the mouse was sated and excluded these trials and any subsequent trials from our analysis, except during the trimming experiments. If a mouse did not reach 240 trials within a session, data from that entire session was excluded. All times reported during a trial were measured from the onset of the response window (0 seconds).

QUANTIFICATION AND STATISTICAL ANALYSIS

All statistical analyses were performed using MATLAB. The analyses performed were ANOVAs, with multiple comparisons and Wilcoxon rank sum. Unless otherwise noted, all tests were two-tailed and all plots with error bars were reported as mean ± SEM. Sample size was not predetermined using power analysis.

Supplementary Material

Refer to Web version on PubMed Central for supplementary material.

Acknowledgements

This work was supported by The New York Stem Cell Foundation and grants from the Arnold and Mabel Beckman Foundation, NINDS grant DP2NS087725-01, the McKnight Foundation, the Simons Foundation Collaboration for the Global Brain award 415569 to I.A.O., and NEI grant K99 EY029758-01 to I.A.O. We thank Dan Feldman and members of the Adesnik lab for a critical reading of the manuscript, Janine Beyer for her invaluable expertise in histology and microscopy and Karthika Gopakumar for technical support.

References

Ahissar E, Assa E, 2016. Perception as a closed-loop convergence process. Elife

Ahissar E, Knutsen PM, 2008. Object localization with whiskers. Biol. Cybern

Andermann ML, Moore CI, 2006. A somatotopic map of vibrissa motion direction within a barrel column. Nat. Neurosci 9, 543–551. [PubMed: 16547511]

Anjum F, Turni H, Mulder PGH, van der Burg J, Brecht M, 2006. Tactile guidance of prey capture in Etruscan shrews. Proc. Natl. Acad. Sci 103, 16544–16549. [PubMed: 17060642]

Arabzadeh E, Petersen RS, Diamond ME, 2003. Encoding of whisker vibration by rat barrel cortex neurons: Implications for texture discrimination. J. Neurosci 23, 9146–9154. [PubMed: 14534248]

Brecht M, Preilowski B, Merzenich MM, 1997. Functional architecture of the mystacial vibrissae. Behav. Brain Res

Brecht M, Roth A, Sakmann B, 2003. Dynamic receptive fields of reconstructed pyramidal cells in layers 3 and 2 of rat somatosensory barrel cortex. J. Physiol 553, 243–265. [PubMed: 12949232]

Brumberg JC, Pinto DJ, Simons DJ, 1996. Spatial gradients and inhibitory summation in the rat whisker barrel system. J. Neurophysiol 76, 130–140. [PubMed: 8836214]

Bruno RM, Khatri V, Land PW, Simons DJ, 2003. Thalamocortical Angular Tuning Domains within Individual Barrels of Rat Somatosensory Cortex. J. Neurosci 23, 9565–9574. [PubMed: 14573536]

Chen JL, Carta S, Soldado-Magraner J, Schneider BL, Helmchen F, 2013. Behaviour-dependent recruitment of long-range projection neurons in somatosensory cortex. Nature 499, 336–340. [PubMed: 23792559]

Chen TW, Wardill TJ, Sun Y, Pulver SR, Renninger SL, Baohan A, Schreiter ER, Kerr RA, Orger MB, Jayaraman V, Looger LL, Svoboda K, Kim DS, 2013. Ultrasensitive fluorescent proteins for imaging neuronal activity. Nature

Curtis JC, Kleinfeld D, 2009. Phase-to-rate transformations encode touch in cortical neurons of a scanning sensorimotor system. Nat. Neurosci 12, 492–501. [PubMed: 19270688]

Diamond ME, Von Heimendahl M, Knutsen PM, Kleinfeld D, Ahissar E, 2008. “Where” and “what” in the whisker sensorimotor system. Nat. Rev. Neurosci 9, 601–612. [PubMed: 18641667]

DiCarlo JJ, Johnson KO, 2000. Spatial and Temporal Structure of Receptive Fields in Primate Somatosensory Area 3b: Effects of Stimulus Scanning Direction and Orientation. J. Neurosci 20, 495–510. [PubMed: 10627625]

Drew PJ, Feldman DE, 2007. Representation of moving wavefronts of whisker deflection in rat somatosensory cortex. J. Neurophysiol 98, 1566–1580. [PubMed: 17567777]

Friedrich J, Zhou P, Paninski L, 2017. Fast online deconvolution of calcium imaging data. PLoS Comput. Biol

Gibson JJ, 1962. Observations on active touch. Psychol. Rev 69, 477–491. [PubMed: 13947730]

Govorunova EG, Sineshchekov OA, Janz R, Liu X, Spudich JL, 2015. Natural light-gated anion channels: A family of microbial rhodopsins for advanced optogenetics. Science (80-.)

Hires SA, Pammer L, Svoboda K, Golomb D, 2013. Tapered whiskers are required for active tactile sensation. Elife

Hong YK, Lacefield CO, Rodgers CC, Bruno RM, 2018. Sensation, movement and learning in the absence of barrel cortex. Nature 561, 542–546. [PubMed: 30224746]

Hsiao S, 2008. Central mechanisms of tactile shape perception. Curr. Opin. Neurobiol 18, 418–424. [PubMed: 18809491]

Hsiao SS, Lane J, Fitzgerald P, 2002. Representation of orientation in the somatosensory system. Behav. Brain Res 135, 93–103. [PubMed: 12356439]

Hutson KA, Masterton RB, 1986. The Sensory Contribution Cortical Barrel October 56.

Isett BR, Feasel SH, Lane MA, Feldman DE, 2018. Slip-Based Coding of Local Shape and Texture in Mouse S1. Neuron 97, 418–433.e5. [PubMed: 29307709]

Jacob V, Le Cam J, Ego-Stengel V, Shulz DE, 2008. Emergent Properties of Tactile Scenes Selectively Activate Barrel Cortex Neurons. Neuron 60, 1112–1125. [PubMed: 19109915]

Jadhav SP, Wolfe J, Feldman DE, 2009. Sparse temporal coding of elementary tactile features during active whisker sensation. Nat. Neurosci

Jones LM, Lee SH, Trageser JC, Simons DJ, Keller A, 2004. Precise temporal responses in whisker trigeminal neurons. J. Neurophysiol 92, 665–668. [PubMed: 14999053]

Kathleen Kelly M, Carvell GE, Kodger JM, Simons DJ, 1999. Sensory loss by selected whisker removal produces immediate disinhibition in the somatosensory cortex of behaving rats. J. Neurosci 19, 9117–9125. [PubMed: 10516329]

Kim J, Erskine A, Cheung JA, Hires SA, 2020. Behavioral and Neural Bases of Tactile Shape Discrimination Learning in Head-Fixed Mice. Neuron

Kleinfeld D, Delaney KR, 1996. Distributed representation of vibrissa movement in the upper layers of somatosensory cortex revealed with voltage-sensitive dyes. J. Comp. Neurol

Kleinfeld D, Deschênes M, 2011. Neuronal basis for object location in the vibrissa scanning sensorimotor system. Neuron

Knutsen PM, Ahissar E, 2009. Orthogonal coding of object location. Trends Neurosci

Knutsen PM, Biess A, Ahissar E, 2008. Vibrissal Kinematics in 3D: Tight Coupling of Azimuth, Elevation, and Torsion across Different Whisking Modes. Neuron

Knutsen PM, Pietr M, Ahissar E, 2006. Haptic object localization in the vibrissal system: Behavior and performance. J. Neurosci

Krupa DJ, Wiest MC, Shuler MG, Laubach M, Nicolelis MAL, 2004. Layer-specific somatosensory cortical activation during active tactile discrimination. Science (80-.) 304, 1989–1992.

Kwon SE, Tsytsarev V, Erzurumlu RS, O'Connor DH, 2018. Organization of orientation-specific whisker deflection responses in layer 2/3 of mouse somatosensory cortex. Neuroscience 368, 46–56. [PubMed: 28827090]

Lavzin M, Rapoport S, Polsky A, Garion L, Schiller J, 2012. Nonlinear dendritic processing determines angular tuning of barrel cortex neurons in vivo. Nature 490, 397–401. [PubMed: 22940864]

Lederman SJ, Klatzky RL, 1987. Lederman&Klatzky1987 Handmovements.pdf. Cogn. Psychol 19, 342–368. [PubMed: 3608405]

Leiser SC, Moxon KA, 2007. Responses of Trigeminal Ganglion Neurons during Natural Whisking Behaviors in the Awake Rat. Neuron 53, 117–133. [PubMed: 17196535]

Mardinly AR, Oldenburg IA, Pégard NC, Sridharan S, Lyall EH, Chesnov K, Brohawn SG, Waller L, Adesnik H, 2018. Precise multi-modal optical control of neural ensemble activity. Nat. Neurosci 21, 881–893. [PubMed: 29713079]

Minnery BS, Simons DJ, 2003. Response properties of whisker-associated trigeminothalamic neurons in rat nucleus principalis. J. Neurophysiol 89, 40–56. [PubMed: 12522158]

O'Connor DH, Peron SP, Huber D, Svoboda K, 2010. Neural activity in barrel cortex underlying vibrissa-based object localization in mice. Neuron 67, 1048–1061. [PubMed: 20869600]

Otchy TM, Wolff SBE, Rhee JY, Pehlevan C, Kawai R, Kempf A, Gobes SMH, Ölveczky BP, 2015. Acute off-target effects of neural circuit manipulations. Nature 528, 358–363. [PubMed: 26649821]

Pachitariu M, Stringer C, Schröder S, Dipoppa M, Rossi LF, Carandini M, Harris KD, 2016. Suite2p: beyond 10,000 neurons with standard two-photon microscopy. bioRxiv

Perrett DI, Rolls ET, Caan W, 1982. Visual neurones responsive to faces in the monkey temporal cortex. Exp. Brain Res

Petersen CCH, 2019. Sensorimotor processing in the rodent barrel cortex. Nat. Rev. Neurosci

Pluta S, Naka A, Veit J, Telian G, Yao L, Hakim R, Taylor D, Adesnik H, 2015. A direct translaminar inhibitory circuit tunes cortical output. Nat. Neurosci 18, 1631–1640. [PubMed: 26414615]

Pluta SR, Lyall EH, Telian GI, Ryapolova-Webb E, Adesnik H, 2017. Surround Integration Organizes a Spatial Map during Active Sensation. Neuron 94, 1220–1233.e5. [PubMed: 28504117]

Polley DB, Rickert JL, Frostig RD, 2005. Whisker-based discrimination of object orientation determined with a rapid training paradigm. Neurobiol. Learn. Mem 83, 134–142. [PubMed: 15721797]

Ramirez A, Pnevmatikakis EA, Merel J, Paninski L, Miller KD, Bruno RM, 2014. Spatiotemporal receptive fields of barrel cortex revealed by reverse correlation of synaptic input. Nat. Neurosci

Sachidhanandam S, Sreenivasan V, Kyriakatos A, Kremer Y, Petersen CCH, 2013. Membrane potential correlates of sensory perception in mouse barrel cortex. Nat. Neurosci

Saig A, Gordon G, Assa E, Arieli A, Ahissar E, 2012. Motor-sensory confluence in tactile perception. J. Neurosci

Simons DJ, 1985. Temporal and spatial integration in the rat SI vibrissa cortex. J. Neurophysiol 54, 615–635. [PubMed: 4045540]

Simons DJ, Carvell GE, 1989. Thalamocortical response transformation in the rat vibrissa/barrel system. J. Neurophysiol

Slotnick B, 2009. A SIMPLE 2-TRANSISTOR TOUCH OR LICK DETECTOR CIRCUIT. J. Exp. Anal. Behav

Sofroniew NJ, Vlasov YA, Hires SA, Freeman J, Svoboda K, 2015. Neural coding in barrel cortex during whisker-guided locomotion. Elife 4, 1–19.

Stüttgen MC, Schwarz C, 2008. Psychophysical and neurometric detection performance under stimulus uncertainty. Nat. Neurosci

Timofeeva E, Lavallée P, Arsenault D, Deschênes M, 2004. Synthesis of multiwhisker-receptive fields in subcortical stations of the vibrissa system. J. Neurophysiol 91, 1510–1515. [PubMed: 14668302]

Vilarchao ME, Estebanez L, Shulz DE, Férézou I, 2018. Supra-barrel Distribution of Directional Tuning for Global Motion in the Mouse Somatosensory Cortex. Cell Rep 22, 3534–3547. [PubMed: 29590621]

Waiblinger C, Brugger D, Schwarz C, 2015. Vibrotactile discrimination in the rat whisker system is based on neuronal coding of instantaneous kinematic cues. Cereb. Cortex 25, 1093–1106. [PubMed: 24169940]

Wekselblatt JB, Flister ED, Piscopo DM, Niell CM, 2016. Large-scale imaging of cortical dynamics during sensory perception and behavior. J. Neurophysiol

Woolsey TA, Van der Loos H, 1970. The structural organization of layer IV in the somatosensory region (S I) of mouse cerebral cortex. Brain Res

Yang H, Kwon SE, Severson KS, O'Connor DH, 2015. Origins of choice-related activity in mouse somatosensory cortex. Nat. Neurosci 19, 127–134. [PubMed: 26642088]

Highlights:

- Mice use multiple whiskers to discriminate object orientation
- Mice learn a generalized object orientation rule, invariant to absolute object location
- Barrel Cortex neurons encodes object orientation by summating across whiskers
- Acute disruption of Barrel Cortex activity impairs performance

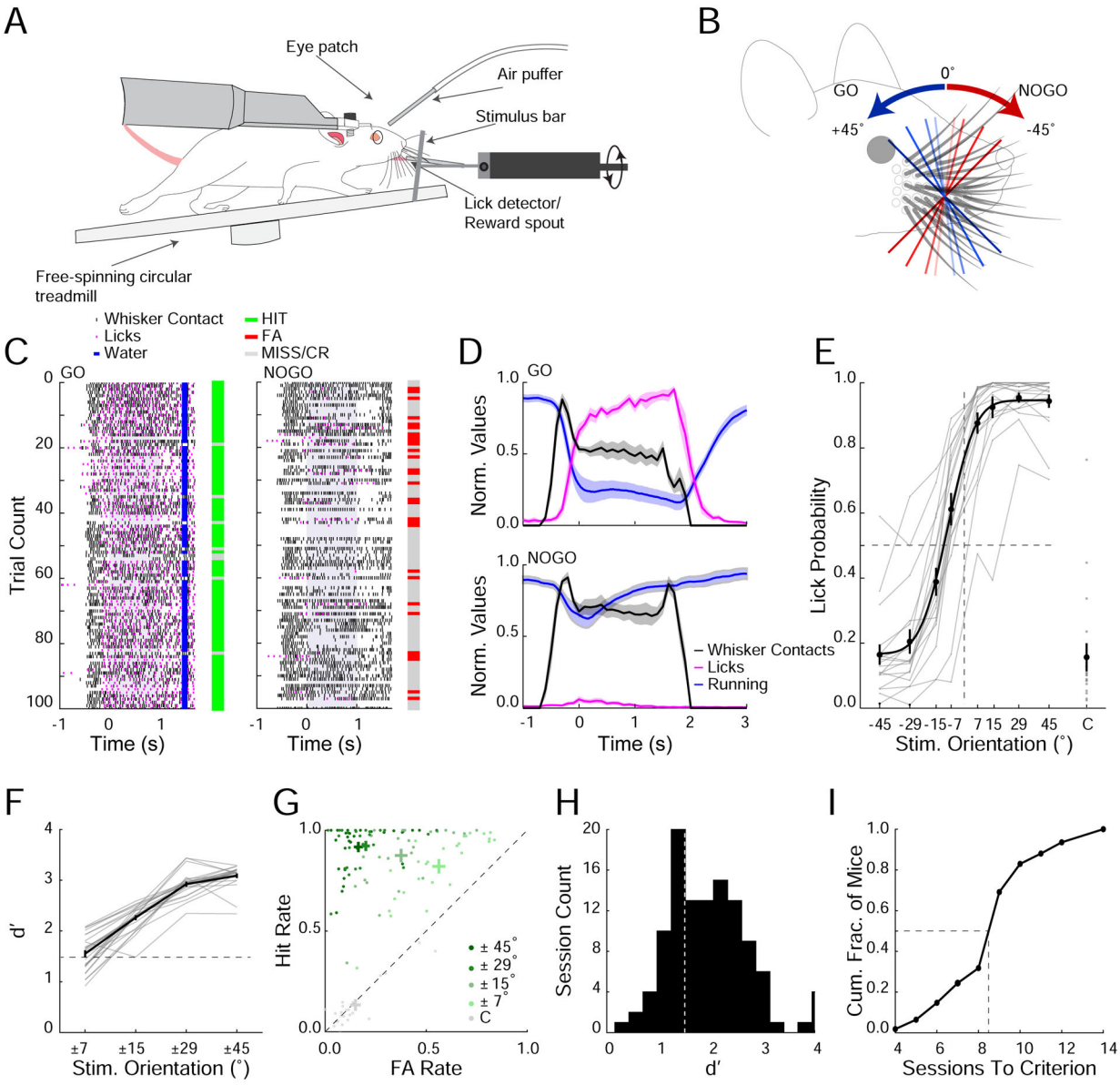

Figure 1. An orientation discrimination task for mice during active haptic sensation

A. Schematic of experimental setup. An orientated stimulus bar is presented unilaterally to the right whisker field of a head-fixed, freely running mouse.

B. Stimulus bar is either positively oriented (GO trials; blue shades) or negatively oriented (NOGO trials; red shades).

C. Raster plot of behavioral during a single example session separated into GO (*left*) and NOGO trials (*right*). The whiskers contact the stimulus bar (black tick marks) as it moves into the whisker field. Time points 0 represents when the bar stops and the start of the 1 second response window (shaded gray). Licks (magenta ticks), reward delivery (blue ticks). Bars to the right of raster plots show performance on each trial (green; Hit, red; FA, gray; CR or Miss).

D. Average normalized running velocity (blue), whisker contacts (black) and lick frequency (magenta) separated into GO trials (*top*) and NOGO trials (*bottom*) for a subset of mice where whisker contact data was collected (n=3 mice, 6 sessions).

E. Psychometric performance curve (n=25 mice, averages from individual mice (gray); group mean ± SEM and fit (black)). Dashed lines represent midpoints for 0° stimulus orientation and 0.5 lick probability. C= catch trial.

F. d' for corresponding orientation pairs (n=25 mice, averages from individual mice (gray); group mean ± SEM (black)). Dashed line represents performance criterion (d'>1.5).

G. Hit and FA rates for all sessions over performance criterion separated into orientation pairs and catch trials (n=25 mice).

H. Distribution of d' values during learning. Dashed line represents performance criterion.

I. Cumulative histogram of the number of sessions to reach performance criterion across mice.

Also see Figure S1–3.

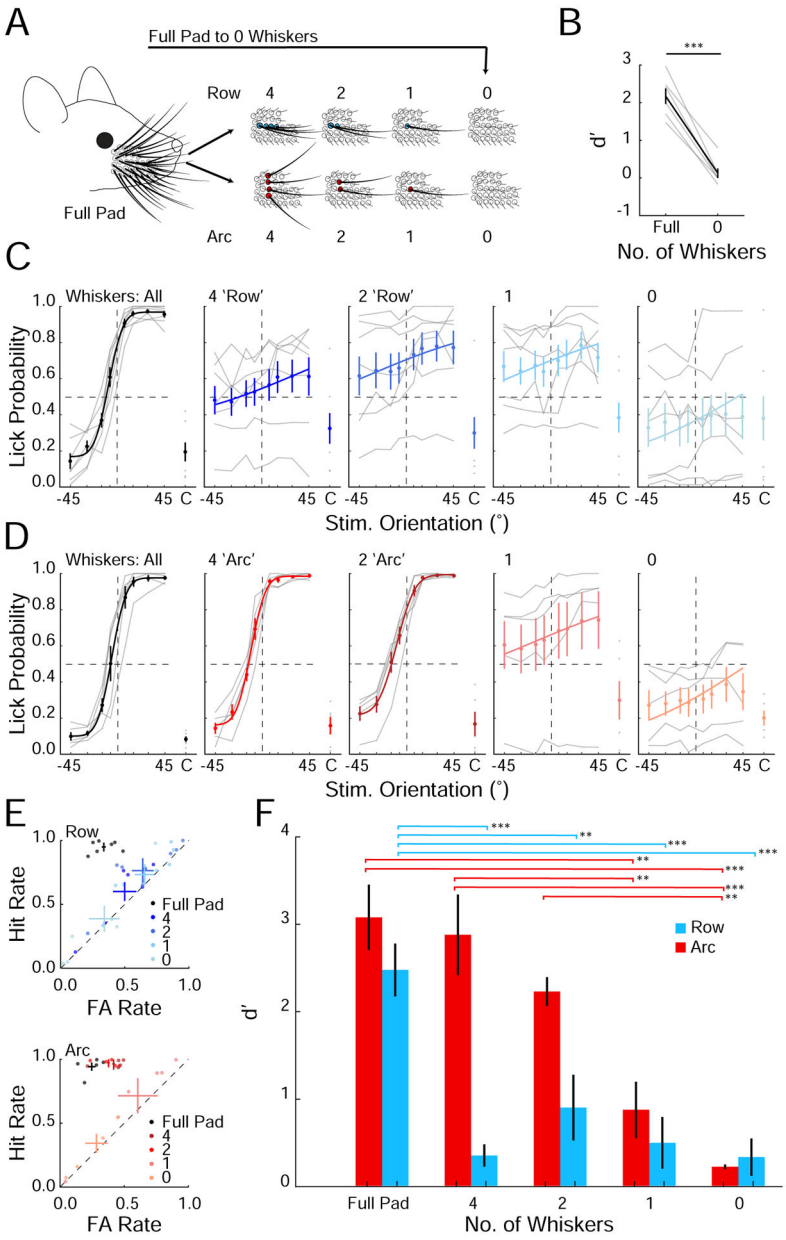

Figure 2. Mice must integrate sensory input from at least two vertically stacked whiskers to discriminate orientations

A. Schematic of the progressive whisker trimming experiment.

B. Performance of mice that was abruptly trimmed from full whisker pad to 0 whiskers (***p<0.001, n=6 mice, rank sum test).

C. Task performance in mice progressively trimmed to a row of whiskers (n=7 mice; averages from individual mice (gray); mean ± SEM and fit (solid colors).

D. As in C) but for mice trimmed to an arc of whiskers (n=5 mice).

E. Hit and FA rates for mice trimmed to a row (*top*) or an arc (*bottom*) of whiskers. Color shade indicates the number of remaining whiskers in each condition. Individual mice (points) and means ± SEM (solid colors).

F. Summary plot of average performance of each group during the progressive trimming paradigm (**p<0.01, ***p<0.001, ANOVA).

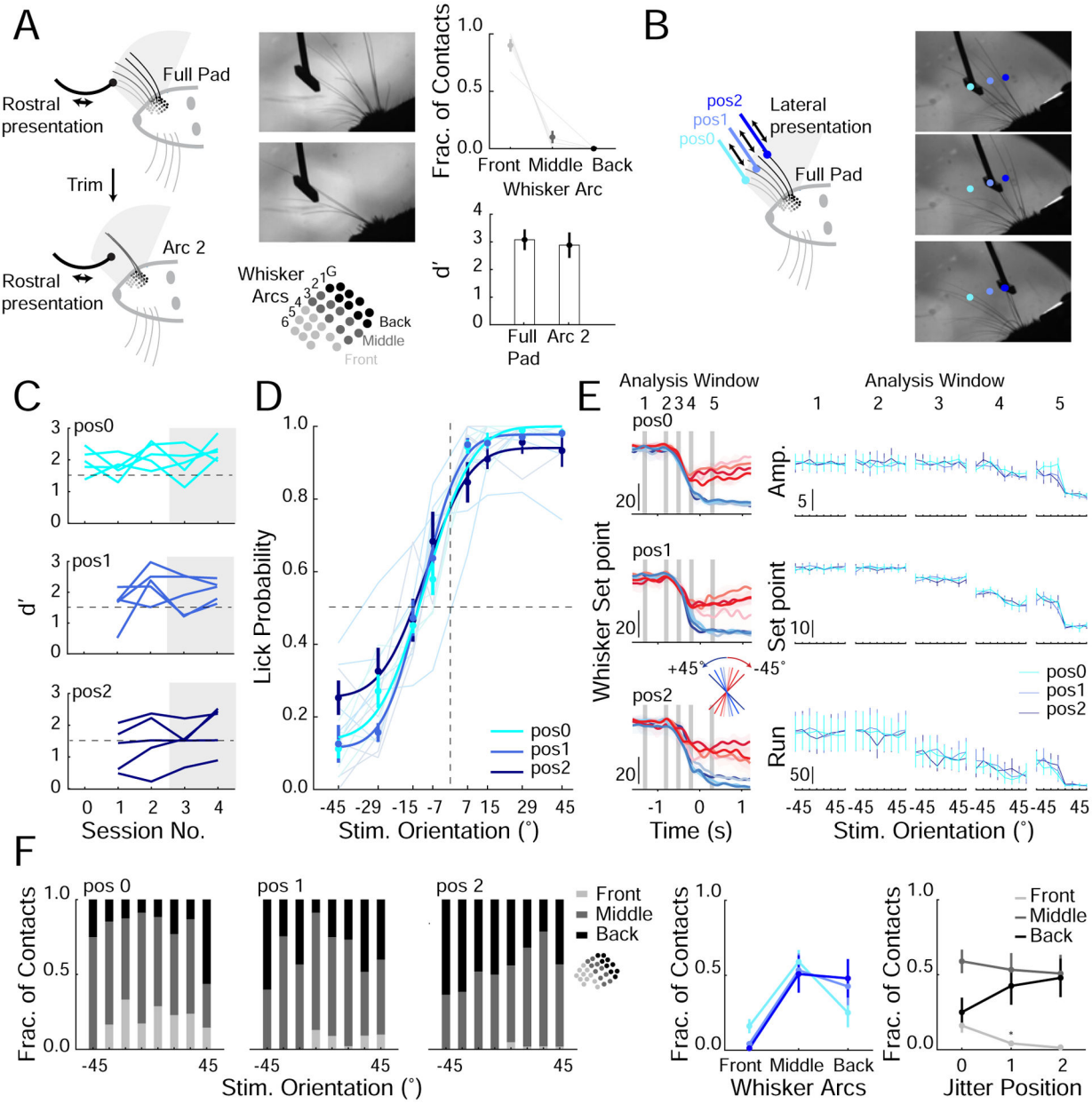

Figure 3. Mice can generalize the orientation discrimination rules to multiple stimulus positions

A. Schematic of mouse using full whisker pad (*top; left*) or an arc of whiskers (*bottom; left*) to perform task, corresponding example frame from high-speed imaging (*middle; top*) and schematic of mouse whisker pad (*middle; bottom*). Distribution of whiskers (front, middle or back) contacting stimulus bar during the decision period with full pad (Right; top, n=3 mice, 3 sessions). Performance with full and arc of whiskers intact (right; *bottom*, n=5 mice replotted from Figure 2F).

B. Schematic of positional jitter experiment (*left*). The stimulus bar was presented laterally to one of three final stationary positions (pos 0, pos 1, pos 2; targeting front, middle and back whiskers respectively). *Right*; example frames of whiskers contacting stimulus bar at each position.

C. d’ for each mouse one day before lateral jitter is introduced (session number 0; stimulus bar presented laterally to one position, pos0) and four days (session number 1–4) separated by each position. Dashed line represents performance criterion.

D. Average psychometric curves from days 3–4 (n=5 mice), averages from individual mice (light colors according to position); group mean ± SEM and fit (solid colors). Dashed lines are 0° stimulus orientation and 0.5 lick probability.

E. *Left*: example average whisker set point separated by stimulus orientation (colored lines) and jitter position (top to bottom; pos0, pos1 and pos2) for a single session. Gray bars represent each analysis window (see Methods and Figure S3). *Right*: mean value during each analysis window for whisker amplitude (amp. (degrees)), whisker set point (degrees) and run velocity (cm/s^2; n=5 mice, ANOVA).

F. *Left*: fraction of contacts with each whisker group for each lateral jitter positions and for each stimulus orientation. *Middle*: average fraction of contacts each whisker group made to the stimulus bar across jitter positions. *Right*: Re-plotted to show fraction of contacts each jitter position received from each whisker group (n=5 mice, *P<0.05, ANOVA).

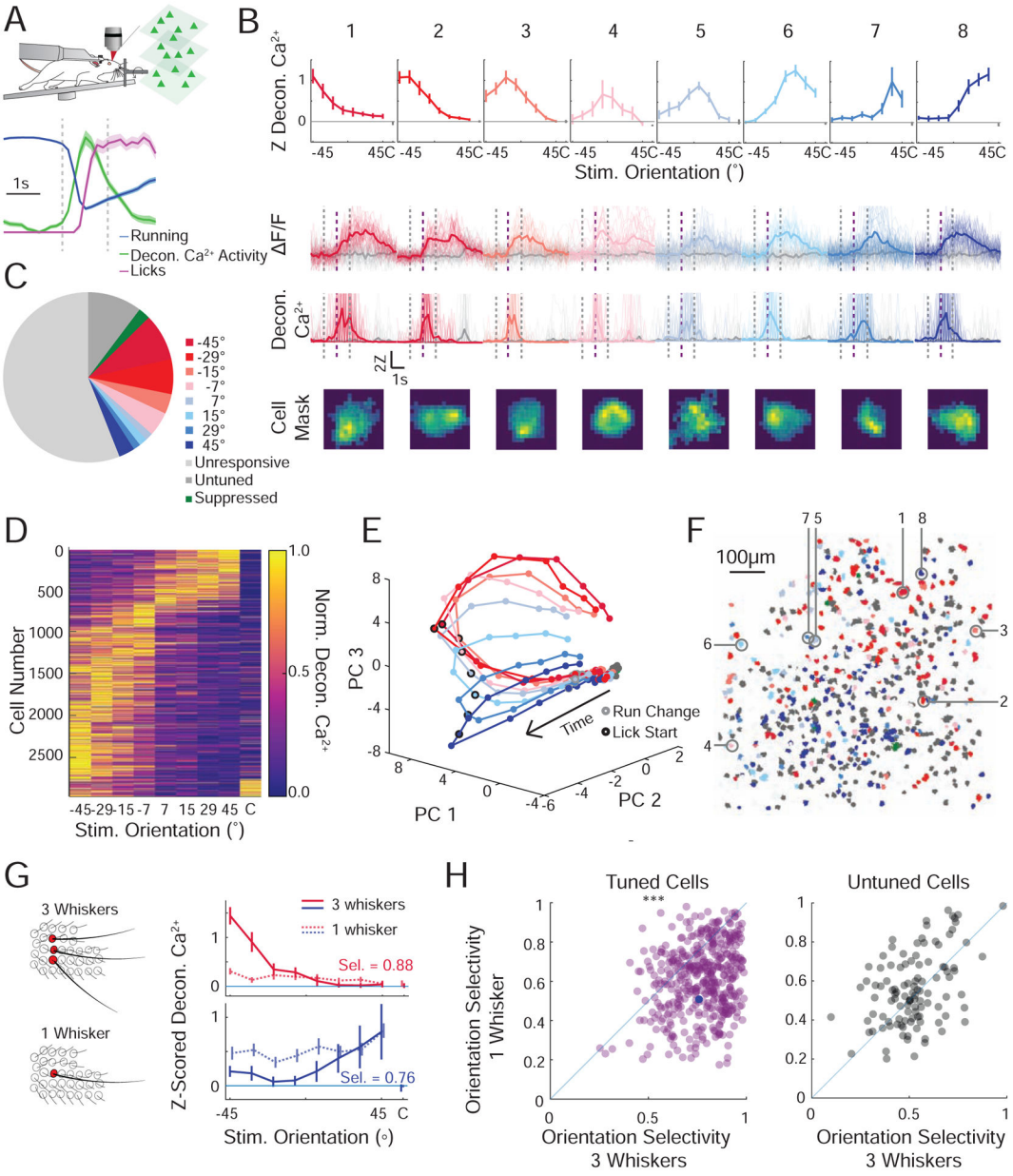

Figure 4. Somatosensory cortical neurons encode each stimulus orientation

A. Schematic of Ca^{2+} imaging experiment. Normalized mean ± SEM for run speed (blue), lick rate (magenta), and deconvolved Ca^{2+} response (all neurons, green). Standard analysis window (vertical dashed lines).

B. *Top:* Mean z-scored deconvolved Ca^{2+} responses of 8 representative neurons from the same field of view, tuned to each of the presented stimuli (color coded to preferred stimulus, mean ±95% confidence interval). *Middle:* Fluorescence response for each neuron during presentation of preferred stimulus (color) or catch trial (gray). Presented as ΔF/F (*above*) or deconvolved Ca^{2+} activity (*below*) (individual trial responses (faint lines), mean response (solid line)). *Bottom:* Weighted pixel mask from raw images. Scalebar 10µm. Standard

analysis window (vertical dashed lines). Lick onset (in GO trials; vertical dashed purple line).

C. Pie chart showing the relative fractions of all imaged neurons that prefer each stimulus orientation (n=10,140 cells, 9 recordings, 4 mice).

D. Cross-validated tuning curves for all significantly tuned cells detected across all mice normalized and sorted by preferred stimulus (determined by half the data that is not shown).

E. Population activity from a representative recording reduced in dimensionality through principal component analysis (PCA). The mean trajectory through PCA space for each oriented stimulus is presented. Each dot is an imaging frame, the time of run deviation (gray circle) and lick onset (black circle) are noted.

F. Stimulus preference map of all neurons recorded in a single recording session; 3 imaging planes are superimposed. Significantly tuned cells are color coded by their preferred orientation (red to blue), untuned but touch-responsive cells (dark gray), unresponsive cells (light gray). The 8 example cells from B are identified.

G. *Left*: Schematic of the trimming experiment. *Right:* Orientation tuning curves for two representative neurons during presentation of stimuli with three intact whiskers in an arc (solid line), and a single remaining whisker (lighter dotted line). Inset: orientation selectivity (Sel.) in the three-whisker condition.

H. Scatter plot of orientation selectivity of neurons before (three whiskers) or after trimming to one whisker. Magenta (*left*), cells that were tuned in the three-whisker condition and responsive in the one whisker condition (n=446 cells, p<3e-41, signed rank test) and gray (*right*), cells that were untuned (aka touch responsive but not tuned) before trimming and responsive (with any tuning) in the one whisker condition (n=110 cells p=0.32). Cells that were unresponsive before or after trimming are not displayed (n=2 mice; 2138 cells). The b*ottom* example neuron from (I) is marked by a solid blue circle.

Also see Figure S4–9 and Movie 1.

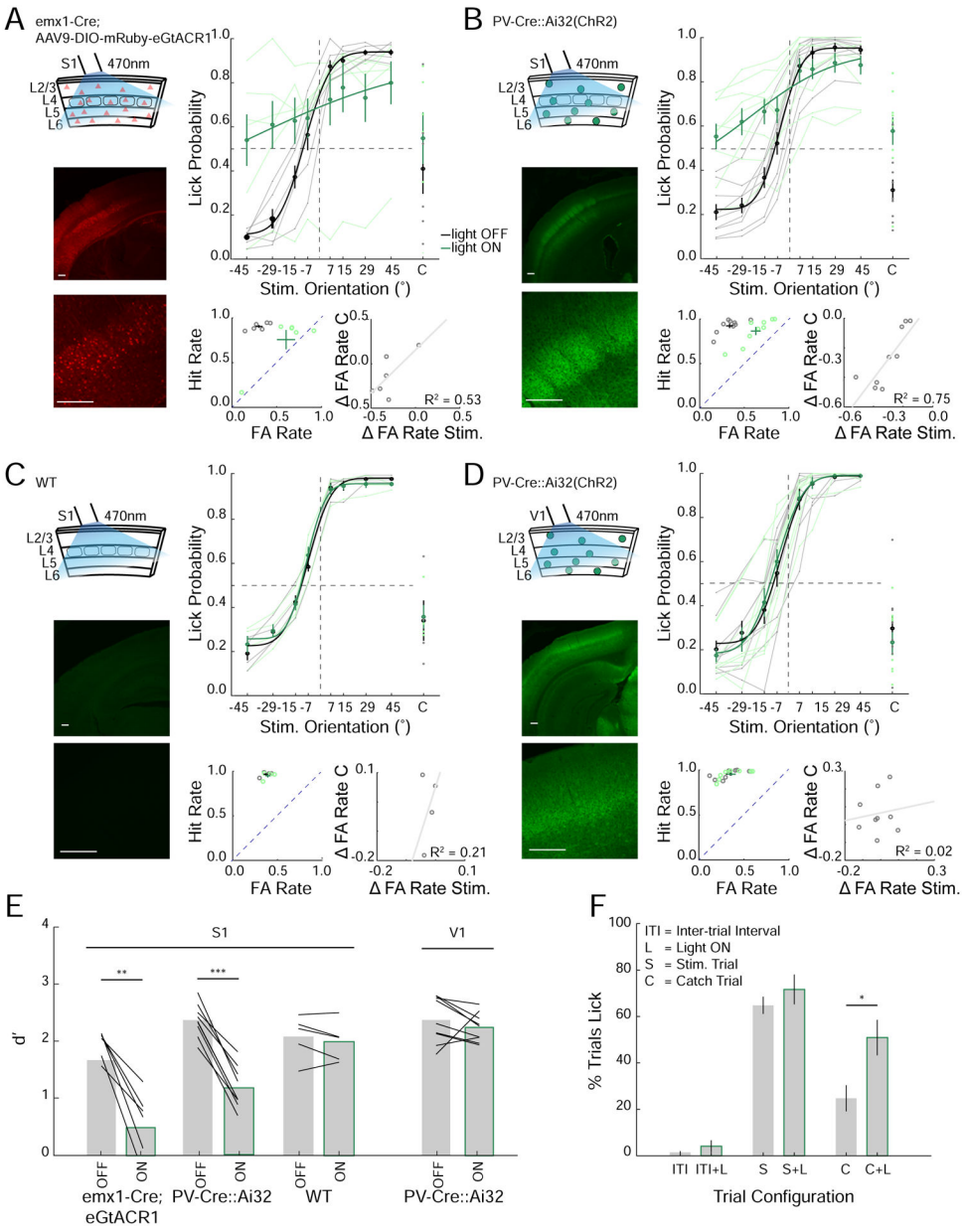

Figure 5. Acute inactivation of the barrel cortex impairs performance in the orientation discrimination task

A. *Left top*: Schematic of optogenetic suppression of S1 via emx1-Cre mice virally expressing GtACR1. *Left bottom*: Confocal image of coronal section through S1 (Scalebar 200μm). *Right top*: Task performance during light off (gray) and light on (green) trials (n=6 mice, average from individual mice (thin lines) and group mean ± SEM and fit (solid lines)). *Right bottom; left*: FA versus Hit rate for each mouse, dashed line represents unity line (light off (gray), light on (green)). *Right bottom; right*: change in FA rate (light on – light off) for stimulus (Stim.) versus catch (C) trials (fit line - linear regression).

B. As in A but for PV-Cre::Ai32(ChR2) in S1 (n=9 mice).

C. As in A, B but for wild type (WT) mice in S1 (n=4 mice).

D. As in A-C but for PV-Cre::Ai32(ChR2) mice where the optogenetic illumination was targeted to the primary visual cortex (V1, n=9 mice).
E. Average d' for each cohort (black lines: individual mice, mean ± SEM, **p<0.01, ***p<0.001, rank sum test).
F. Quantification of licking of PV-Cre::Ai32 mice with optogenetic silencing over S1 during the inter-trial interval (ITI), stimulus trial (S) or catch trial (C) with (L) and without light on (For S and C conditions; n=11 mice, 22 sessions, for ITI conditions 3 mice, 5 sessions, *p<0.05, rank sum test).

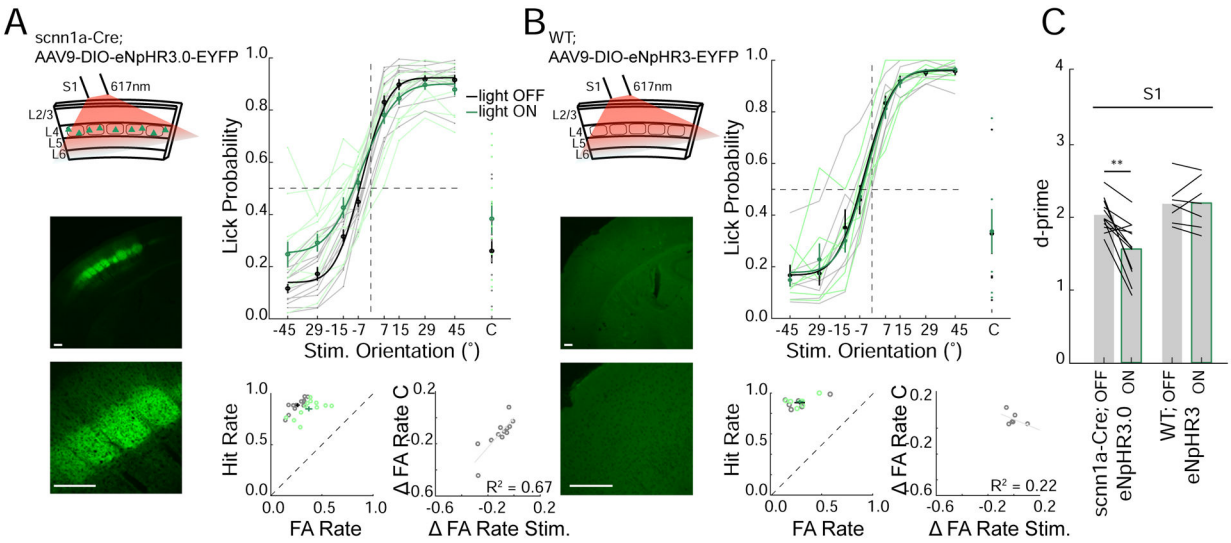

Figure 6. Selective optogenetic suppression of layer 4 excitatory neurons decrease performance in the object discrimination task

A. *Left top*: Schematic of optogenetic suppression of S1 layer 4 excitatory neurons via scnn1a-Cre mice virally expressing eNpHR3. *Left bottom*: Confocal image of coronal section through S1 (Scalebar 200μm). *Right top*: Task performance during light off (gray) and light on (green) trials (n=12 mice, average from individual mice (thin lines) and group mean ± SEM and fit (solid lines)). *Right bottom; left*: FA versus Hit rate for each mouse, dashed line represents unity line (light off (gray) light on (green)). *Right bottom; right*: change in FA rate (light on – light off) for stimulus (Stim.) versus catch (C) trials (fit line - linear regression).

B. As in A but for Cre-negative (WT) control mice virally injected with eNpHR3.0 in S1 (n=5 mice).

C. Average d' for light off and light on conditions (black lines; individual mice, mean ± SEM **p<0.01, rank sum test).

KEY RESOURCES TABLE

REAGENT or RESOURCE	SOURCE	IDENTIFIER
Bacterial and virus strains		
AAV9-CAG-DIO-NLS-mRuby3-IRES-ST-eGtACR1-ST.WPRE.SV40	Mardinly et al 2018	RRID:Addgene_109048
AAV9-EFla-DIO-eNPHR3.0-EYFP-WPRE-hGH	Gradinaru et al 2010	RRID:Addgene_26966
AAV9-syn-FLEX-GCaMP6s-WPRE.SV40	Chen et al 2013	RRID:Addgene_100845
Experimental models: organisms/strains		
Mouse: CD-1	Charles River	RRID:MGI:5659424
Mouse: PV-IRES-Cre	Jackson Laboratory	RRID:IMSR_Jax:030218
Mouse: RSL-Channelrhodopsin2/eYFP(Ai32)	Jackson Laboratory	RRID:IMSR_Jax:024109
Mouse: Rosa-LSL-ChR2	Jackson Laboratory	RRID:IMSR_JAX:012569
Mouse: B6. 129S2-Emx1 $^{tm1(cre)Krj}$/J	Jackson Laboratory	RRID:IMSR_JAX:005628
Mouse: B6;C3-Tg(Scnn1a-cre)3Aibs/J	Jackson Laboratory	RRID:IMSR_JAX:009613
Mouse: B6;DBA-Tg(tetO-GCaMP6s)2Niell/J	Jackson Laboratory	RRID:IMSR_JAX:024742
Mouse: Camk2a-tTA	Jackson Laboratory	RRID:IMSR_JAX:003010
Software and algorithms		
MATLAB	MathWorks	RRID:SCR_001622
Suite2p	Pachitariu et al 2017	RRID:SCR_016434
OASIS	Friedrich et al 2017	RRID:SCR_007385
Janelia Whisker Tracker	Clack et al 2012	https://wiki.janelia.org/wiki/display/MyersLab/Whisker+Tracking
ScanImage	Vidrio Inc.	RRID:SCR_014307
Adobe Illustrator	Adobe	RRID:SCR_010279
Other		
Arduino Due/Mega 2560	Arduino	A000067
Two-photon microscope	Sutter MOM, Sutter Inc.	MOM-RES-SIP
920nm laser	Coherent Chameleon	
Stepper Motor (Nema 8 & Nema 17)	Sparkfun	ROB-10846/1204
Solenoid Valve	Neptube Research Inc.	161K011
Incremental encoder	US Digital	H5
T-cube LED Driver	Thorlabs	LEDD1B
Fiber Coupled LED – Blue 470nm	Thorlabs	
Fiber Coupled LED – orange 617nm	Thorlabs	M617F2
Basler camera acA2000–340km	Edmund Optics NT58–257	acA2000–340km
Frame Grabber	Silicon Software	
Piezo bender	Noliac Systems	NDR6110–100
20X Objective	Olympus	XLUMPlanFLN N20X-PFH